APPENDIX B

GEOCHEMICAL AND HYDROLOGICAL DATA FOR FLOW BELOW THE REPOSITORY (RESPONSE TO RT 3.02, TSPAI 3.24, AND GEN 1.01 (COMMENT 106))

Note Regarding the Status of Supporting Technical Information

This document was prepared using the most current information available at the time of its development. This Technical Basis Document and its appendices providing Key Technical Issue Agreement responses that were prepared using preliminary or draft information reflect the status of the Yucca Mountain Project's scientific and design bases at the time of submittal. In some cases this involved the use of draft Analysis and Model Reports (AMRs) and other draft references whose contents may change with time. Information that evolves through subsequent revisions of the AMRs and other references will be reflected in the License Application (LA) as the approved analyses of record at the time of LA submittal. Consequently, the Project will not routinely update either this Technical Basis Document or its Key Technical Issue Agreement appendices to reflect changes in the supporting references prior to submittal of the LA.

APPENDIX B

GEOCHEMICAL AND HYDROLOGICAL DATA FOR FLOW BELOW THE REPOSITORY (RESPONSE TO RT 3.02, TSPAI 3.24, AND GEN 1.01 (COMMENT 106))

This appendix provides a response for Key Technical Issue (KTI) agreement entitled Radionuclide Transport (RT) 3.02, Total System Performance Assessment and Integration (TSPAI) 3.24, and general agreement (GEN) 1.01 (Comment 106). These agreements relate to providing geochemical and hydrological data used for support of the flow field below the repository.

B.1 KEY TECHNICAL ISSUE AGREEMENTS

B.1.1 RT 3.02, TSPAI 3.24, and GEN 1.01 (Comment 106)

Agreement RT 3.02 was reached during the U.S. Nuclear Regulatory Commission (NRC)/U.S. Department of Energy (DOE) Technical Exchange and Management Meeting on Radionuclide Transport held December 5 to 7, 2000 (Reamer and Williams 2000), in Berkeley, California. RT subissue 3, radionuclide transport through fractured rock, was discussed at that meeting.

At that meeting, the NRC expressed the need for additional support for establishing the length of the flow path to which fracture transport conditions apply (Reamer and Williams 2000) and cautioned that when lacking a geostatistical analysis, estimation of flow length should err on the side of conservatism. The DOE responded that path lengths are generally the shortest between the repository and water table, with the exception where flow is diverted by perched water and that sensitivity analyses showed that the transport time is not significantly affected by the path length.

TSPAI 3.24 was reached during the NRC/DOE Technical Exchange and Management Meeting on Total System Performance Assessment and Integration held August 6 through 10, 2001, in Las Vegas, Nevada (Reamer and Gil 2001a). TSPAI subissue 3, model abstraction, was discussed at that meeting.

In the discussion of the model abstraction pertaining to the flow paths in the unsaturated zone, the NRC commented that there are insufficient water potential and geochemical data to support the flow fields predicted by the unsaturated zone site-scale model in the CHn, Prow Pass, and Bullfrog units below the repository (Cornell 2001). Of particular concern to the NRC staff was the estimated fraction of water that may travel significant distances through permeable nonwelded vitric tuff matrix versus the fraction that may be laterally diverted atop layers of low-permeability zeolitized or moderate to densely welded tuff to fast pathways to the water table (e.g., through faults). The focus of this concern is on areas where no perched water is predicted and unsaturated zones in the lower CHn, Prow Pass, and Bullfrog units below the perched water. In addition, the NRC staff requested a basis for the use of current hydraulic properties, rather than thermally perturbed properties; specifically, zeolitization of the nonwelded, unaltered Tptpv1, Tptb1, and upper Tac may be caused by the thermal pulse. The NRC staff also noted that statistics of flow percent in faults versus matrix and fractures that are

relevant to the entire unsaturated zone model domain may not reflect flow regimes below the repository footprint. In response, the DOE proposed to address the uncertainty in the CHn flow through sensitivity studies for radionuclide transport for a range of potential CHn flow conditions. In addition, the DOE proposed to update the unsaturated zone flow models and submodels to include the flow path and flow field for moisture tension and geochemical data.

Agreement GEN 1.01 was reached during the NRC/DOE Technical Exchange and Management Meeting on Range of Thermal Operating Temperatures, held September 18 to 19, 2001 (Reamer and Gil 2001b). At that meeting, the NRC provided additional comments, resulting in GEN 1.01 (Comment 106), which relates to TSPAI 3.24.

The wording of these agreements is as follows:

RT 3.02

> Provide the analysis of geochemical data used for support of the flow field below the repository. DOE will provide the analysis of geochemical data used for support of the fluid flow patterns in the AMR Unsaturated Zone Flow Models and Submodels, available to the NRC in FY 2002.

TSPAI 3.24[1]

> Provide the analysis of geochemical and hydrological data (water content, water potential, and temperature) used for support of the flow field below the repository, particularly in the Calico Hills, Prow Pass, and Bullfrog hydrostratigraphic layers. Demonstrate that potential bypassing of matrix flow pathways below the area of the proposed repository, as opposed to the entire site-scale model area, is adequately incorporated for performance assessment, or provide supporting analyses that the uncertainties are adequately included in the TSPA (UZ2.3.3).
>
> DOE will provide an analysis of available geochemical and hydrological data (water content, water potential, and temperature) used for support of the flow field below the repository, particularly in the Calico Hills, Prow Pass, and Bullfrog hydrostratigraphic layers. The analyses will demonstrate that potential bypassing of matrix flow pathways below the area of the proposed repository, as opposed to the entire site-scale model area, is adequately incorporated for performance assessment, or provide supporting analyses that the uncertainties are adequately included in the TSPA. These analyses will be documented in the Unsaturated Zone Flow Models and Submodels AMR (MDL-NBS-HS-000006), In-Situ Field Testing of Processes AMR (ANL-NBS-HS-000005), and Calibrated Properties Model AMR (MDL-NBS-HS-000003) expected to be available to NRC in FY 2003.

[1] UZ2.3.3 in this agreement refers to item 3.3 of NRC integrated subissue UZ2 (NRC 2002, Table 1.1-2). This item addresses NRC's concern that water potential and geochemical data to support flow fields are insufficient.

GEN 1.01 (Comment 106)

> The DOE needs to provide additional technical bases for excluding uncertainties in infiltrating water compositions that are associated with the coupled THC model from TSPA analyses. The DOE has not adequately demonstrated that the initial water compositions used in sensitivity studies in the coupled THC models are appropriate and bounding (Chapters 3 and 6). What are the technical bases for selecting these particular water compositions selected for the analysis? Do they differ from one another in significant ways? Do they represent the full range of ground water compositions that have been collected and measured from Yucca Mountain and vicinity? How do variations in infiltrating water composition influence the In-Drift salts/evaporation models?

DOE Initial Response to GEN 1.01 (Comment 106)[2]

> As stated on page 6-15, the Alcove-5 water compositions selected for most of the THC seepage modeling work were "the only available nearly full suites of analyses from a repository host unit" at the time the modeling work was initiated. In Section 6.3.1.5.3, additional simulations using UZ-14 perched water are presented. The UZ-14 perched-water composition is a good example of a reliable analysis significantly different from the Alcove-5 pore-water analyses. Additional work is planned for the next couple of years to collect additional pore-water samples from the TSw in the Exploratory Studies Facility, analyze the data, and use the data to improve the THC seepage model to better predict seepage chemistry consistent with TSPAI 3.24.
>
> Sensitivity to starting water composition on evaporative chemical evolution is documented in Section 6.3.3.5.1.1 of SSPA Vol. 1. These studies take seven different known water compositions and evaporate them using the In-drift precipitates salts model. The results of these sensitivities indicate that for 7 waters there are three possible chemical divides that the brine generation follows. The first representing waters like J-13, perched water, water from the single heater test, and water from the drift scale test evolve to a sodium nitrate brine. The second set representative of the Topopah Spring pore water takes the brine towards calcium (or magnesium) chloride brine. The third set derived from the Rev 00 DST THC seepage abstraction results and associated grout modified waters that contain more sulfates than calcium. These three different brines would give different relative humidity thresholds for brine formation on the waste package and have different boiling point elevations for any brine associated with the waste package.

This appendix provides the initial DOE response to agreements RT 3.02, TSPAI 3.24, and GEN 1.01 (Comment 106).

[2] The specific section or page number referral cited below is from *FY01 Supplemental Science and Performance Analyses, Volume 1: Scientific Bases and Analyses* (BSC 2001a).

B.1.2 Related Key Technical Issue Agreements

KTI agreements RT 3.02, TSPAI 3.24, and GEN 1.01 (Comment 106) are related to RT 1.01. RT 1.01 addresses the justification of the approach for modeling flow through the CHnv units (i.e., dominant matrix flow). In comparison, RT 3.02, TSPAI 3.24, and GEN 1.01 (Comment 106) concern the general use of geochemical and hydrological data in the calibration and validation of the unsaturated zone flow field for all hydrostratigraphic units below the repository. The response to agreement RT 1.01 is provided in Appendix A of this technical basis document.

B.2 RELEVANCE TO REPOSITORY PERFORMANCE

Flow and transport through the unsaturated zone plays an important part in the assessment of postclosure performance. Since fracture flow dominates radionuclide transport in most unsaturated hydrostratigraphic units (BSC 2003a, Section 6), the documentation of all geochemical and hydrological data that are used to support the flow fields below the repository is important for confidence building in the TSPA-LA transport calculations.

B.3 RESPONSE

KTI agreements RT 3.02, TSPAI 3.24, and GEN 1.01 (Comment 106) pertain to the documentation and use of subsurface hydrological, temperature, and geochemical data for support of the flow-field concept below the repository.

The unsaturated zone (UZ) flow and transport models under discussion include the mountain-scale flow model (called the UZ flow model), temperature model, and geochemical models (chloride transport model, calcite model, and strontium isotope model) (BSC 2003b). All the models (except for the calcite model) were three-dimensional models. The UZ flow model investigates flow processes using hydrological data (saturation, water potential, and perched water data). The TSPA-LA flow fields were generated from the UZ flow model, which uses the property set of the PTn with and without lateral flow diversion within the PTn (BSC 2003b, Sections 6.2.5, 6.6.2, 6.6.3). All other models support the UZ flow model through the investigation of ambient-thermal and geochemical processes using temperature and geochemical data.

No new data sets were used in the 2003 revision of the UZ flow model (BSC 2003b) at the repository horizon (the ESF and ECRB Cross Drift). There were some new samplings in the ECRB Cross Drift for pore-water chloride and other composition measurements; however the new chloride data are considered to be redundant, in the sense that they cover locations that have the previously available chloride data.

The UZ flow model was supported by various data collected from boreholes, the Exploratory Studies Facility (ESF), and Enhanced Characterization of the Repository Block (ECRB) Cross Drift before 2000 (KTI agreement RT 3.02 was established in a December 2000 meeting (Reamer and Williams 2000)). The field- and laboratory-measured data include hydrological data (saturation, water potential, and perched water), pneumatic pressure data, temperature and geochemical data (chloride, calcite, and strontium). However, only the boreholes drilled below the repository horizon can provide data (except pneumatic pressure data) that directly supports the flow and transport modeling below the repository. Most of the borehole data had been

available and used in the initial version of the *UZ Flow Models and Submodels* (CRWMS M&O 2000). Since then, the supporting database has not expanded noticeably. In the 2003 revision of the *UZ Flow Models and Submodels* (BSC 2003b), no new data regarding saturation, water potential, and perched water were available for the UZ flow model. A total of three more boreholes have available temperature measurements for the ambient thermal model, with removal of two previous boreholes (UE-25 NRG#5 and USW SD-7) and addition of five boreholes (USW H-4, USW H-5, UE-25 WT#18, UE-25 UZ#4, and UE-25 UZ#7a). The chloride transport model utilized chloride data from 10 more boreholes, compared to the initial one borehole (UE-25 UZ#16). Calcite data remain the same in the calcite model (UE-25 WT#24, USW SD-6, and USW G-2). A new strontium isotope model for two boreholes (USW SD-9 and UE-25 SD-12) and the ECRB Cross Drift was added.

Responses to the KTI agreements are organized into six parts. Section B.3.1 briefly discusses the hydrological properties of the welded and nonwelded tuffs as follows: (1) the conceptual model of layered representation of tuff hydrological properties in the UZ flow model; (2) the subsurface hydrological properties calibrated from a one-dimensional flow model; (3) the nonwelded vitric tuffs within the CHn units and its approximation as a single matrix porosity medium; and (4) the reasoning that hydrological properties used in the UZ temperature model do not include thermally perturbed properties. Section B.3.2 discusses flow below the repository, including perched water, percolation rates, matrix, fractures, and fracture fluxes. Section B.3.3 deals with saturation and water potential hydrological data. Section B.3.4 discusses the temperature data. Section B.3.5 presents the analyses of chloride, strontium and calcite geochemical data that were used to calibrate and verify the UZ flow model. Section B.3.6 contains the response to the comment regarding the compositions of infiltration water in the thermal-hydrological-chemical seepage model (BSC 2003c). The model results of the UZ flow model are shown to be consistent with the various field-measured data below the repository. The technical basis for these responses is provided in Section B.4.

The first five parts of this section (Sections B.3.1 through B.3.5) pertain to the response to KTI agreement TSPAI 3.24, with the response to KTI agreement 3.02 provided in the fifth part (Section B.3.5). The sixth part (Section B.3.6) provides the response to GEN 1.01 (Comment 106).

B.3.1 Calibrated Properties of Tuffs below the Repository

The nonwelded and welded tuffs in the Yucca Mountain show varying degrees of fracture development. They are generally classified into separate identifiable hydrogeological units according to their hydrological properties (BSC 2003d; BSC 2003e). The hydrogeologic layers below the repository include the middle and lower parts of TSw, CHn (zeolitic or vitric), Prow Pass, and Bullfrog.

In the UZ flow model, the dual-permeability method (a continuum approach) is used for describing flow and transport: the fractured tuffs are modeled as fracture and matrix continua. Each matrix and fracture continuum has its own hydrological properties (matrix permeabilities, matrix van Genuchten water-potential relationship (α and m); fracture permeability, van Genuchten parameters α and m, and an active-fracture model parameter γ). The fracture and matrix hydrogeologic properties used for the three-dimensional mountain-scale UZ flow model

were calibrated using one-dimensional inversion of field-measured saturation, water potential, and gas pressure data (BSC 2003d, Section 6.3). Fracture permeability and van Genuchten *m* are assigned data from laboratory and field measurements and were not further calibrated, because they are relatively insensitive to simulated matrix-saturation and water-potential distributions (BSC 2003d, Section 6.3.2, Table 4).

Matrix properties were calibrated with hydrological data. The amount of hydrological data available for model calibrations varies. Water-potential data used for the property calibration were collected from three boreholes. Continuous and rather evenly distributed saturation measurements were collected from as many as 13 boreholes from the ground surface to the bottom. Locations within and below the repository were represented as well as those above. The amount of water-potential data is much less than that of saturation (BSC 2003d, Section 6.3, Table 9). Water-potential data from the borehole samples were measured in the laboratory. These measurements are very sensitive to alterations in moisture content, and therefore samples must be adequately preserved. Because of the experimental difficulty of obtaining uncompromised water potential measurements, fewer reliable water potential data are available for calibration.

Fracture permeabilities are calibrated by matching the pneumatic pressure data that correspond to a mountain-scale process. Pneumatic pressure data were collected from four boreholes (BSC 2003d, Table 7) at locations above the repository only. However, it makes sense that the pneumatic pressure measurements were made only at shallower depths, since the response of pneumatic pressures at locations below the repository is expected to be less sensitive and of less importance.

Calibration of fault properties was performed using data from a borehole (UE-25 UZ#7a) near the Ghost Dance fault, located near the east boundary of the repository block. This fault is an important hydrogeological feature, since it is a potential flow path for receiving lateral flows along eastward tilted layer interfaces (BSC 2003d, Section 6.3.4). Data (including saturation, water potential, and gas pressure data) were collected from the surface to the repository horizon. Locations below the repository have no data support.

The CHn vitric layers are modeled as a single-porosity matrix in the UZ flow model (BSC 2003b) from the consideration of the high permeable matrix. This is supported by observations of matrix-flow dominance shown in the Busted Butte field test of the nonwelded vitric layer and the ESF Alcove 4 test bed in the PTn layer, which has similar porous matrix properties with the CHn vitric layers (BSC 2003f, Sections 6.7 and 6.13).

Parameter uncertainties in calibrated parameter data (BSC 2003d, Section 6.4.1) come from sources such as model simplifications, scale effects, and infiltration-rate uncertainty. Infiltration rate contributes to parameter uncertainty because the fluxes in the unsaturated zone are largely determined by the upper boundary conditions. Using the three infiltration scenarios (present-day mean infiltration and infiltrations with lower and upper bounds) for parameter calibration captures this uncertainty (BSC 2003d, Section 6.4).

The UZ flow model utilizes properties from the *Calibrated Properties Model* (BSC 2003d). Hydrological data used in the one-dimensional inversion calibration are described in the

Calibrated Properties Model (BSC 2003d, Section 4.1.2). More discussion of calibrated properties for the KTI agreements is given Section B.4.1.

B.3.2 Flow Fields below the Repository

In the UZ flow model, flows in fractured tuffs are predominantly vertical flows, in response to gravity. However, below the repository horizon, such flow patterns are altered in the vitric zones within the CHn units, in the central and southern portions of the model domain, because of high matrix permeability and eastward-tilted layering structure. The base-case flow fields at the water table show lateral flow of several hundreds of meters to the east, in the area directly below the southern repository (BSC 2003b, Section 6.6.3). In the northern part of the domain, the flow fields are less sensitive to the calibrated properties. Because of the impact of perched water and zeolitic units, flow is mainly focused into major faults.

Fracture flow is dominant both at the repository horizon and at the water table. In fact, fracture flow consists of more than 90% to 95% of the total percolation fluxes at the repository level, whereas it is about 70% to 80% at the water table. On the other hand, fault flow percentage increases from about 30% to 40% at the repository to about 60% at the water table, reflecting the conditions imposed by matrix-permeability reduction in the zeolitic zones in the CHn units, perched water formation, and lateral flow into the major faults.

In the general discussion of the flow fields, the water table was determined from the present-day measured data. The flow fields with a raised water table (in future climates) are addressed in Section B.4.2.

B.3.3 Hydrological Data for the Unsaturated Zone Flow Model

The UZ flow model uses perched-water, saturation, and water-potential data measured from the field (BSC 2003b, Sections 6 and 7). Because the flow below the repository is studied as an integrated part in the UZ flow model, the relevant hydrological property data at and below the repository are discussed together with those above the repository. Similarly, the same format is used in discussions of the temperature and geochemical data in the following sections.

Perched-water location data from seven boreholes were used in simulating the occurrences of perched water in the UZ flow model. Because the calibrated properties were derived based on one-dimensional inversion of field-measured data and are incapable of reproducing either perched-water formation or lateral flow, they are further adjusted in the UZ flow model to simulate the occurrence of perched water.

The saturation data used in the calibration of the UZ flow model come from seven boreholes (five of which were also used in the *Calibrated Properties Model* (BSC 2003d)). Water potential data were from three boreholes (UE-25 SD-12 is also used in the *Calibrated Properties Model* (BSC 2003d)). Overall, the water-potential data for the TSw (and TCw) units are scarce or not available. The TSw units were characterized by water-potential data locally distributed in the first few hundred meters from the entrance of the ECRB Cross Drift. Generally, no data are available from the repository down to near the top of the CHn units.

Model results for perched water, saturation, and water potential match well with the observed data (BSC 2003b, Section 6.6.3). The hydrological data used in the calibration and validation are described in the *UZ Flow Models and Submodels* (BSC 2003b, Section 4.1). More relevant discussion regarding the hydrological data for the KTI agreements is provided in Section B.4.3.

B.3.4 Temperature Data for the Unsaturated Zone Flow Model

Model analyses of temperature data provide an independent examination of percolation fluxes simulated by the UZ flow model. The UZ temperature model uses temperature data measured from a total of nine surface-based deep boreholes (BSC 2003b, Sections 6.3 and 7.7). The borehole temperature data cover the depths below the repository as well as those above it. Model results compare well with the observed data of the boreholes.

The data used in the calibration and validation of the unsaturated zone model are described in the *UZ Flow Models and Submodels* (BSC 2003b, Sections 4.1, 6.3, and 7.7; BSC 2001b). Section B.4.4 provides more relevant discussion regarding the KTI agreements.

B.3.5 Geochemical Data for the Unsaturated Zone Flow Model

Chloride and strontium concentrations in pore waters, as well as calcite data were used for calibration and validation of the UZ flow model. Conceptual model for UZ chloride transport was based on the infiltration boundary, established using chloride fluxes, determined by the precipitation fluxes and the concentration in precipitation. The match of the simulated chloride concentrations to the field-measured pore-water concentration provides information regarding past infiltration. Similarly, in the simulation of strontium in the unsaturated zone, strontium input at the surface came from precipitation. Modeled strontium concentrations are compared to measured values to derive information related to infiltration. Data analyses of precipitated calcite in the unsaturated zone also provide information to constrain the infiltration flux. Downward water flows in the unsaturated zone interact with the geothermal gradient, causing the calcite to precipitate from percolating waters (BSC 2003b, Section 7.9.2).

Chloride concentrations were collected from various places, including 11 boreholes, the ECRB Cross Drift, and the ESF. The ECRB Cross Drift is relatively well sampled. However, chloride data from the ESF are restricted to three discrete locations. Moreover, the available chloride data are typically incomplete along a vertical profile through the unsaturated zone. Specifically, borehole chloride data for the TSw layers (as well as TCw layers above the repository) are usually missing. Chloride data are rare in the lower TSw units above CHn (i.e., chloride data correspond to the depth interval from the repository to the perched water). The limited chloride data in the TSw (and TCw) units results from TSw (and TCw) welded tuffs having a very low water content, such that collecting enough rock mass to extract enough pore water for chemical analysis is experimentally difficult. Strontium data are available from USW SD-9 and UE-25 SD-12 and the ECRB Cross Drift. Calcite data are limited to UE-25 WT#24, USW SD-6, and USW G-2.

The model results for chloride, strontium, and calcite models also are in good agreement with the observed data. Chloride and strontium concentrations and calcite abundance data used in the UZ geochemical models are described in the *UZ Flow Models and Submodels* (BSC 2003b,

Sections 6.5 and 7.10, respectively). Additional discussion of the geochemical data can be found in Section B.4.5.

B.3.6 Water Compositions in the Coupled Thermal-Hydrological-Chemical Seepage Models

GEN 1.01 (Comment 106) relates to KTI agreement RT 3.02, regarding water compositions selected to represent infiltrating water related to the coupled thermal-hydrological-chemical seepage models (BSC 2003c).

In the initial 2000 version of the *Drift-Scale Coupled Processes (DST and THC Seepage) Models* (BSC 2003c, Section 6.2.2.1), the availability of infiltrating water data was limited to three pore-water samples collected from the highly fractured middle nonlithophysal zone (Tptpmn) geologic unit in Alcove 5, near the Drift Scale Test. Since then, a series of pore-water samples from repository host units have been collected and analyzed in the ECRB Cross Drift and in boreholes USW SD-9 and USW NRG-7/7a (BSC 2003c, Section 6.2.2.1). In the 2003 revised version of the coupled thermal-hydrological-chemical seepage models (BSC 2003c), the selection pool of water composition data waters includes pore waters in the repository horizon, perched water, and saturated zone waters (J-13 well water). A total of five types of infiltrating waters are chosen, with preference given to actual pore waters from unsaturated regions within or above the repository units and exclusion of the perched water and saturated zone water (BSC 2003c, Section 6.2.2.1). The choice of input water composition also takes into consideration the natural variability of pore-water compositions in the repository units. The selected five types of infiltrating waters are expected to show diverse brine developments under evaporation. Corrosive brine calcium chloride and other less corrosive brines are expected to develop in addition to sodium chloride brine.

However, since these new samples were mainly collected from the ECRB Cross Drift, the spatial coverage of these data is too small to derive a probability of occurrence for any of these pore-water compositions.

Waters such as those from USW UZ-14 pore water and J-13 are excluded because they appear dramatically different from pore waters in the repository units, even though they are seemingly end-members of waters from Yucca Mountain and the vicinity. However, this end-member type of water with low pore-water concentrations (with very low (Ca+Mg)/(Na+K) ratio) may exist in the repository horizon, as revealed in a recent finding of pore water with very low chloride concentrations. These low concentrations of chloride are similar to those of J-13 water and may have occurred in the ESF fracture or fault zones where bomb-pulse ^{36}Cl was found (Lu et al. 2003, Section 4.4). Under evaporation conditions, the water from such dilute concentrations is likely to develop into sodium chloride brine or other brines less deleterious than calcium chloride.

Overall, given the limitation in sample numbers and the question of their representativeness, the five infiltrating waters still constitute a reasonable and appropriate selection of water compositions.

B.3.7 Summary of Response

In summary, a significant amount of several kinds of data, including hydrological, temperature, and geochemical data, has been collected to characterize mountain-scale flow. Most of these data were collected from boreholes, with the ECRB Cross Drift being a second source (for water-potential data as well as chloride- and strontium- concentration data). The ESF serves as a minor source. In the UZ flow model and temperature and geochemical models, the model results are demonstrated to be consistent with both field-measured and laboratory data.

A large amount of saturation and temperature data has been collected from surface-based boreholes. Locations below the repository in these boreholes are generally well characterized by saturation and temperature data. Saturation data from surface-based boreholes for locations both above and below the repository horizon provide good spatial coverage—from as many as 13 boreholes used in the one-dimensional property calibration and seven boreholes used in the UZ flow model (five of which were also used in the property calibration) (BSC 2003d). Temperature data were collected from as many as nine surface-based deep boreholes. The temperature boreholes are well represented in the model domain, and the data are rather evenly distributed above and below the repository.

Borehole water-potential data have also been gathered. In the existing borehole water potential data from three boreholes, there are limited samples from location immediately below the repository of the TSw units (from the repository to the top of the CHn). The water potential data for the TSw units were represented by field data locally distributed over a span of a few hundred meters in the ECRB Cross Drift.

Fault properties were calibrated from inversion using saturation and water potential data from one borehole (UE-25 UZ#7a). The data were collected from the regions extending from the surface to the repository horizon. Data for calibration fault properties below the repository is currently not available.

Geochemical data (chloride and strontium concentrations and calcite) are used in the UZ flow and transport model. The strontium data were collected from the ECRB Cross Drift and two boreholes, whereas calcite data were collected from three surface-based boreholes.

Chloride data were used as natural tracers in the UZ transport model. Chloride data were collected from the ESF, ECRB Cross Drift, and 11 boreholes have pore-water chloride data. Locations in boreholes from the repository to the top of the CHn units have limited chloride data, because previous studies have had difficulty in obtaining enough pore water for chemical analysis, owing to the low water contents in the TSw (and TCw) nonwelded tuffs.

Regarding GEN 106 (Comment 106), the selection of the five types of infiltrating data is based on samples collected mainly from the ECRB Cross Drift. Considering the limited amount of data available for characterizing the pore water, the selection represented a reasonable approximation. The water types are expected to develop corrosive calcium chloride and other less-corrosive brines on evaporation, in addition to sodium chloride. The probability of the occurrences of these five types of waters is unknown, because the amount of available data is not large enough to derive the spatial variability of the water samples. The water types (W4 and

W6) may not represent end-member pore waters typical of low concentrations. Very low water concentrations typical of the J-13 well water may have occurred in the repository horizon.

The information in this report is responsive to agreements RT 3.02 and TSPAI 3.24 and GEN 1.01 (Comment 106), made between the DOE and the NRC. The report contains the information that DOE considers necessary for the NRC to review for closure of these agreements.

B.4 BASIS FOR THE RESPONSE

This section provides the basis for the responses to KTI agreement RT 3.02 (Section B.4.5), TSPAI 3.24 (Sections B.4.1 to B.4.5), and GEN 1.01 (Comment 106) regarding the composition of infiltration waters in the thermal-hydrological-chemical seepage model.

In simulating flow and transport within the fractured tuffs in the Yucca Mountain UZ, the dual-permeability modeling method (a continuum approach) is used. It considers global flow occurring not only between fractures, but also between matrix gridblocks, as well as the interflow between fractures and matrix. In this approach, each gridblock of the primary mesh is divided into two gridblocks, one for fracture and the other for matrix, and connected to each other. Correspondingly, the matrix and fracture continua have their own hydrological properties. The relevant discussion of the advantage of using dual-permeability method in the unsaturated zone model can be found in *Calibrated Properties Model* (BSC 2003d, Section 6.1).

B.4.1 Hydrogeologic Layers and Hydrological Properties

The volcanic welded or nonwelded tuffs at Yucca Mountain occur in layers and show variable degrees of fracturing. In the dual-continuum approach of the UZ flow model, the fractured tuffs are described as both fracture and matrix continua, except for the CHn vitric units below the repository, which are treated as a single-porosity matrix only. This is because the CHn vitric units have relatively high matrix permeabilities and low fracture densities, resulting in the dominance of matrix flow.

B.4.1.1 Hydrogeologic Layers

Hydrological properties of Yucca Mountain tuffs are different from layer to layer. But within one hydrogeological layer, the properties (referred to as layer average properties) are homogeneous, except where faulting or variable alteration (e.g., zeolitization) is present. The hydrogeological layers at and below the repository are listed in Table B-1. Specifically, lying below the repository are the TSw hydrostratigraphic layers represented by tsw38 to tsw39, CHn represented by ch1 to ch6, Prow Pass represented by pp4 to pp1, and Crater Flat undifferentiated (Bullfrog) represented by bf3 to bf2 (BSC 2003b, Section 6.1). A typical geologic profile along a vertical east-west transect is illustrated in Figure B-1. The figure also shows the repository horizon from about 1,000 to 1,100 m in elevation, which is at the same level as the ESF and the ECRB Cross Drift.

Table B-1. Selected Layers at and below the Repository Showing Geologic Framework Model 2000 Lithostratigraphy, Unsaturated Zone Model Layer, and Hydrogeologic Unit Correlation Used in the Unsaturated Zone Flow Model

Major Unit (Montazer and Wilson 1984)	Lithostratigraphic Nomenclature (BSC 2002)	Unsaturated Zone Model Grid Layer[a] (BSC 2003e)	Hydrogeologic Unit (Flint 1998)
Topopah Spring welded (TSw)	Tptrl, Tptf	tsw33	TUL
	Tptpul, RHHtop		
	Tptpmn	tsw34	TMN
	Tptpll	tsw35	TLL
	Tptpln	tsw36	TM2 (upper 2/3 of Tptpln)
		tsw37	TM1 (lower 1/3 of Tptpln)
	Tptpv3	tsw38	PV3
	Tptpv2	tsw39 (vit, zeo)	PV2
Calico Hills nonwelded (CHn)	Tptpv1	ch1 (vit, zeo)	BT1 or BT1*a* (altered)
	Tpbt1		
	Tac (Calico)	ch2 (vit, zeo)	CHV (vitric) Or CHZ (zeolitic)
		ch3 (vit, zeo)	
		ch4 (vit, zeo)	
		ch5 (vit, zeo)	
	Tacbt (Calicobt)	ch6 (vit, zeo)	BT
	Tcpuv (Prowuv)	pp4	PP4 (zeolitic)
	Tcpuc (Prowuc)	pp3	PP3 (devitrified)
	Tcpmd (Prowmd)	pp2	PP2 (devitrified)
	Tcplc (Prowlc)		
	Tcplv (Prowlv)	pp1	PP1 (zeolitic)
	Tcpbt (Prowbt)		
	Tcbuv (Bullfroguv)		
Crater Flat undifferentiated (CFu)	Tcbuc (Bullfroguc)	bf3	BF3 (welded)
	Tcbmd (Bullfrogmd)		
	Tcblc (Bullfroglc)		
	Tcblv (Bullfroglv)	bf2	BF2 (nonwelded)
	Tcbbt (Bullfrogbt)		
	Tctuv (Tramuv)		
	Tctuc (Tramuc)	tr3	Not Available
	Tctmd (Trammd)		
	Tctlc (Tramlc)		
	Tctlv (Tramlv)	tr2	Not Available
	Tctbt (Trambt) and below		

Source: BSC 2003b, Table 6.1-1 (modified).

NOTE: [a] Defined as a rock material type, represented by the code name, for gridblocks belonging to the rock unit.

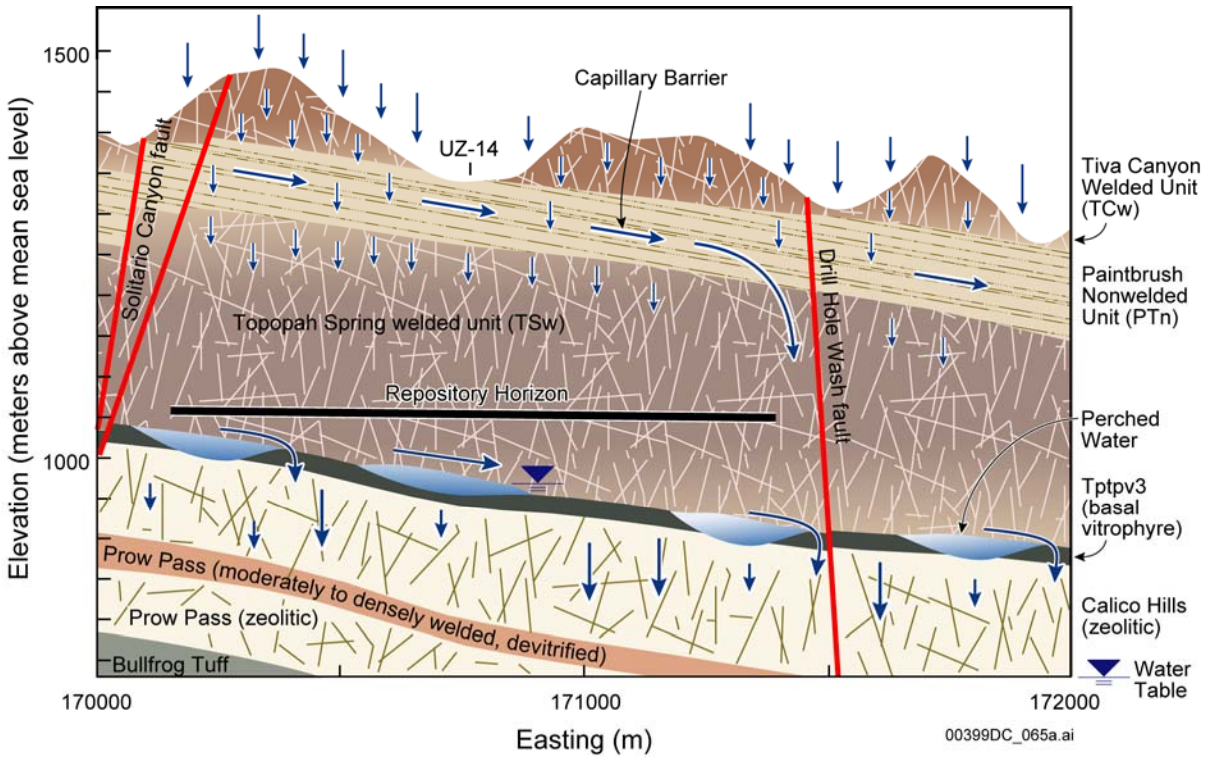

Source: BSC 2003b, Figure 6.2-1.

Figure B-1. Schematic Diagram Showing a Typical Geologic Profile along a Vertical East–West Transect and the Conceptualized Flow Processes and Effects of Capillary Barriers, Major Faults, and Perched-Water Zones within the Unsaturated Zone Flow Model Domain

B.4.1.2 Calibrated Hydrological Properties and Uncertainties

The hydrological properties of the layers were calibrated using one-dimensional inversion of saturation, water-potential data, and gas pressure data (BSC 2003d, Section 6.3). The model report entitled *Calibrated Properties Model* (BSC 2003d) provides the basic input parameter sets of fractures and rock matrix for modeling efforts in the *UZ Flow Model and Submodels* (BSC 2003b). In the *Calibrated Properties Model* (BSC 2003d), the data used for one-dimensional calibration of drift-scale properties from each borehole are listed in Table B-2, and their locations are plotted in Figure B-2. In the drift-scale parameters, the matrix saturation used for the inversion corresponds to 13 surface-based boreholes, and water-potential data is from three boreholes (Table B-2 and Figure B-2). Pneumatic pressure data used for one-dimensional inversion come from four boreholes (BSC 2003d, Table 7), where the gas pressure data were generally taken at or above the repository horizon. Pressure data below the repository are not available. Generally speaking, saturation was sufficiently measured along the boreholes both above and below the repository (BSC 2003d). However, water-potential data are scarce, especially for the TSw layers below the repository.

Table B-2. Data Used for One-Dimensional Calibration of Drift-Scale Properties from Each Borehole

Borehole	Matrix Liquid Saturation (core)	Matrix Liquid Water Potential (*in situ*)
USW NRG-6		4
USW SD-6	4	
USW SD-7	4	
USW SD-9	4	
UE-25 SD-12		4
UE-25 UZ#4		4
USW UZ-14	4	
UE-25 UZ#16	4	
USW UZ-N11	4	
USW UZ-N31	4	
USW UZ-N33	4	
USW UZ-N37	4	
USW UZ-N53	4	
USW UZ-N57	4	
USW UZ-N61	4	
USW WT-24	4	

Source: BSC 2003d, Table 9 (modified).

The scale dependence of matrix permeability properties is assumed to be limited to a relatively small scale associated with the spacing between relatively large fractures (BSC 2003d, Section 6.3). However, drift-scale fracture permeabilities, determined from air-injection tests, cannot be applied to mountain-scale modeling because of the scale difference. Mountain-scale fracture permeabilities are calibrated with the pneumatic pressure data measured in surface borehole UE-25 SD-12 (BSC 2003d, Section 6.3.3).

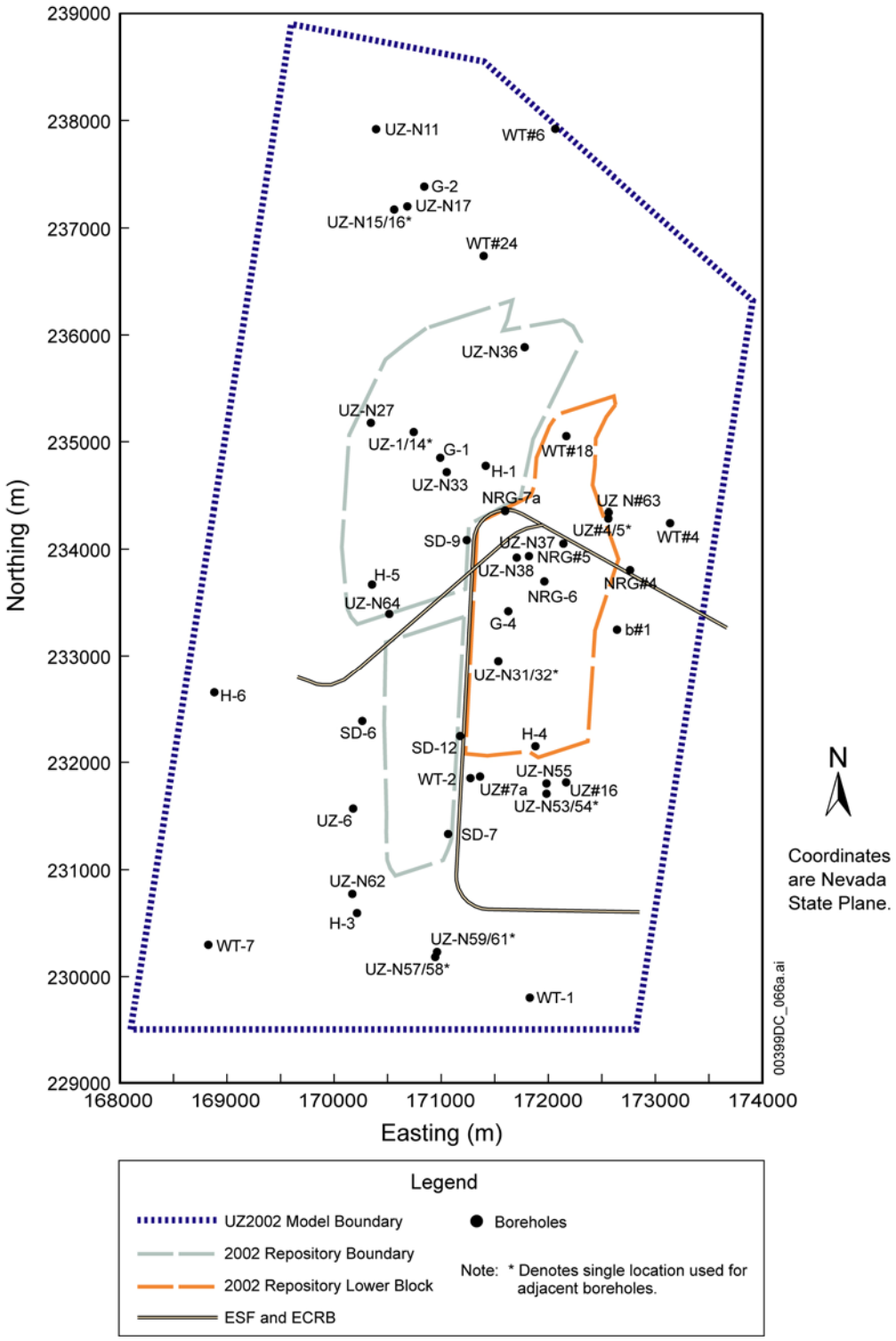

Source: BSC 2003e, Figure 1b.

Figure B-2. Locations of Boreholes in the Property Calibrations

Faults are modeled as vertical or near-vertical planes in the UZ flow model. Generally, high vertical permeability and low capillary forces are expected within the faults (BSC 2003d, Section

6.3.4). The fault properties were generalized from the inversion of hydrological data from borehole UE-25 UZ#7a, which cuts through the Ghost Dance fault. Borehole UE-25 UZ#7a represents the most complete data set from within a fault zone. Saturation, water potential, and pneumatic data are available from the surface down into the repository horizon in the TSw units (BSC 2003d, Table 16, Figures 9 and 10). Data related to water flow in faults below the repository are not available.

The uncertainty in the calibration of hydrological properties is addressed in BSC (2003d, Section 6.4.1). Uncertainty comes from simplification of the one-dimensional conceptual model. For example, one-dimensional models are used for calibrating drift-scale and mountain-scale property sets. Parameter uncertainty in the parameter calibration would result from model simplifications. As a result, lateral flow behavior in the unsaturated zone may not be captured by property sets determined from one-dimensional models. Infiltration-rate uncertainty also contributes to parameter uncertainty, because flow processes in the unsaturated zone are largely determined by upper-boundary conditions. Using the three infiltration scenarios (present-day mean infiltration scenario as base case, along with infiltrations with lower bound and upper bound) for the parameter calibration documented in the calibrated properties captures this uncertainty. In addition, scale effects are a well-known source of parameter uncertainty. This is especially true for determination of the unsaturated zone model parameters. For example, matrix parameters are measured in the unsaturated zone at core scale on the order of several centimeters, whereas in the unsaturated zone flow and transport model, numerical gridblocks are on the order of a few meters to hundreds of meters.

B.4.1.3 Conceptualization of Matrix Flow in Calico Hills Nonwelded Vitric Units

The hydrogeologic layers are usually simulated as dual continua in the UZ flow model. Because the welded tuffs are characterized by low matrix permeability and considerable fracture development, liquid flow occurs predominantly in fractures, with the matrix mainly serving as liquid storage. However, in contrast, the nonwelded vitric layers in the CHn units below the repository have relatively high matrix permeabilities and low fracture densities, leading to predominant matrix flow.

The vitric portions of the CHn units and the lower part of the TSw units occur below the repository. The vitric layers occur in the tsw39, ch1, ch2, ch3, ch4, ch5, and ch6. They are located in the southwest portion of the model domain (BSC 2003e, Section 6.6.3). Vitric tuffs are subject to alteration to zeolite under suitable hydrological conditions (i.e., closeness to water table). The vitric tuffs are considered to be complementary to the abundance of zeolite, so that the vitric-zeolitic regions can be determined by the absence or presence of zeolite contents. However, there is insufficient zeolite x-ray diffraction data to effectively determine the vitric-zeolitic regions within the CHn units. The boundaries of vitric and zeolitic regions were selected using the results of saturated permeability data (BSC 2003e, Assumption 4), measured rock-property data for boreholes within the unsaturated zone model area (BSC 2003e, Assumption 5), and the location of faults with significant vertical offset (BSC 2003e, Assumption 6; Section 6.6.3).

These CHn vitric units are conceptualized and treated as a single-porosity matrix only in the *Unsaturated Zone Flow Model* (BSC 2003b, Section 6.1.2). The effect of fractures in the flow

model within the CHn vitric zones is considered negligible. The conceptual model is supported by observation from the tracer tests in Busted Butte (BSC 2003f). The tests conducted at Busted Butte, in the vitric layers of the upper CHn, show that flow took place in the matrix but not in fractures, even though fractures are present. This observation was made under testing conditions with liquid-release rates much faster than ambient flow conditions (BSC 2003f, Section 6.13).

Corroborative evidence for matrix flow dominance is also found in the field testing at the ESF Alcove 4, which reveals that the PTn units have a significant dampening effect on fracture flow because of matrix imbibition of water flowing along the fracture (BSC 2003f, Section 6.7). The observations for ESF Alcove 4 and Busted Butte are comparable and underscored by the fact that both the CHn vitric units and the PTn have relatively high matrix permeability.

B.4.1.4 Current Hydraulic Properties and Thermally Perturbed Properties

The UZ flow model uses the hydraulic properties calibrated in the *Calibrated Properties Model* (BSC 2003d), rather than thermally perturbed properties. (The mountain-scale thermal modeling is performed in the *Mountain-Scale Coupled Processes (TH/THC/THM)* (BSC 2003g).) This is because on the mountain-scale domain, according to long-term analyses, the effects of thermal loading on flow and transport properties are expected to be small (BSC 2003g, Section 6.1.6).

During the first few years of the thermal-loading period, thermal effects may have a significant impact on thermal-hydrological processes only at or near drifts. Many of the temperature-dependent properties, such as fluid density, viscosity, and specific enthalpy, are incorporated in the formulation of the thermal-hydrological mountain-scale model (BSC 2003g, Section 6.1.6). However, thermal effects on rock properties (such as permeability, relative permeability, and relationship between capillary pressure and liquid saturation) are ignored, because of the limitations of available field data and constitutive relations to describe these phenomena. Moreover, these effects are considered negligible when compared to the uncertainty of the rock properties existing in the collected data (BSC 2003g, Section 6.1.6).

B.4.2 Flow Fields below the Repository and Rising of Water Table

Flow fields are generated for the TSPA-LA calculations from the UZ flow model (BSC 2003b) using the property sets of the PTn with and without lateral flow diversion in the PTn. Accordingly, the base-case flow model uses the property set of the PTn that would favor lateral flow diversion; the alternative model uses the property set of the PTn that would not likely cause flow diversion (BSC 2003b, Sections 6.2.5, 6.6.2, and 6.6.3) (Table B-3).

In the UZ flow model, infiltration is applied at the surface input boundary. Corresponding climate scenarios for infiltration considered in the UZ flow model include present-day (modern) and future monsoonal and glacial climates. Infiltration under each climate scenario is quantified through a mean, lower-, and upper-bound infiltration rate (Table B-3). The uncertainty in the infiltration rates as a boundary condition of the UZ flow model is accordingly addressed. Infiltration under present-day climate and mean infiltration scenario is used in discussing the analyses of the observed data for the KTI agreements. Other climate scenarios are described here for sensitivity analysis and to address the issue of the water table rising (in future climates).

Table B-3. Present-Day, Monsoon, and Glacial Infiltration Scenarios in Unsaturated Zone Flow Model

Scenario Notations	Scenarios
preq_uA preq_uB	Modern upper
preq_mA preq_mB	Modern mean
preq_lA preq_lB	Modern low
monq_uA monq_uB	Monsoon upper
monq_mA monq_mB	Monsoon mean
monq_lA monq_lB	Monsoon low
Glaq_uA Glaq_uB	Glacial upper
Glaq_mA Glaq_mB	Glacial mean
Glaq_lA Glaq_lB	Glacial low

Source: BSC 2003b, Sections 6.2.5, 6.6.2, and 6.6.3.

NOTE: The upper case "A" denotes the base-case model property set used by the corresponding flow model that would favor lateral flow diversion. The upper case "B" denotes the alternative model, in which the property set of the PTn would not likely cause flow diversion. The lower-case letter l (before the upper case A or B) stands for lower bound infiltration, m for mean infiltration, and u for upper bound infiltration scenario.

B.4.2.1 Flow Fields below the Repository

Flow at and below the repository can be illustrated through percolation fluxes, using present-day infiltration. Figures B-3 and B-4 show the percolation flux at the repository layer and at the water table for the present-day mean infiltration scenario of the base-case model.

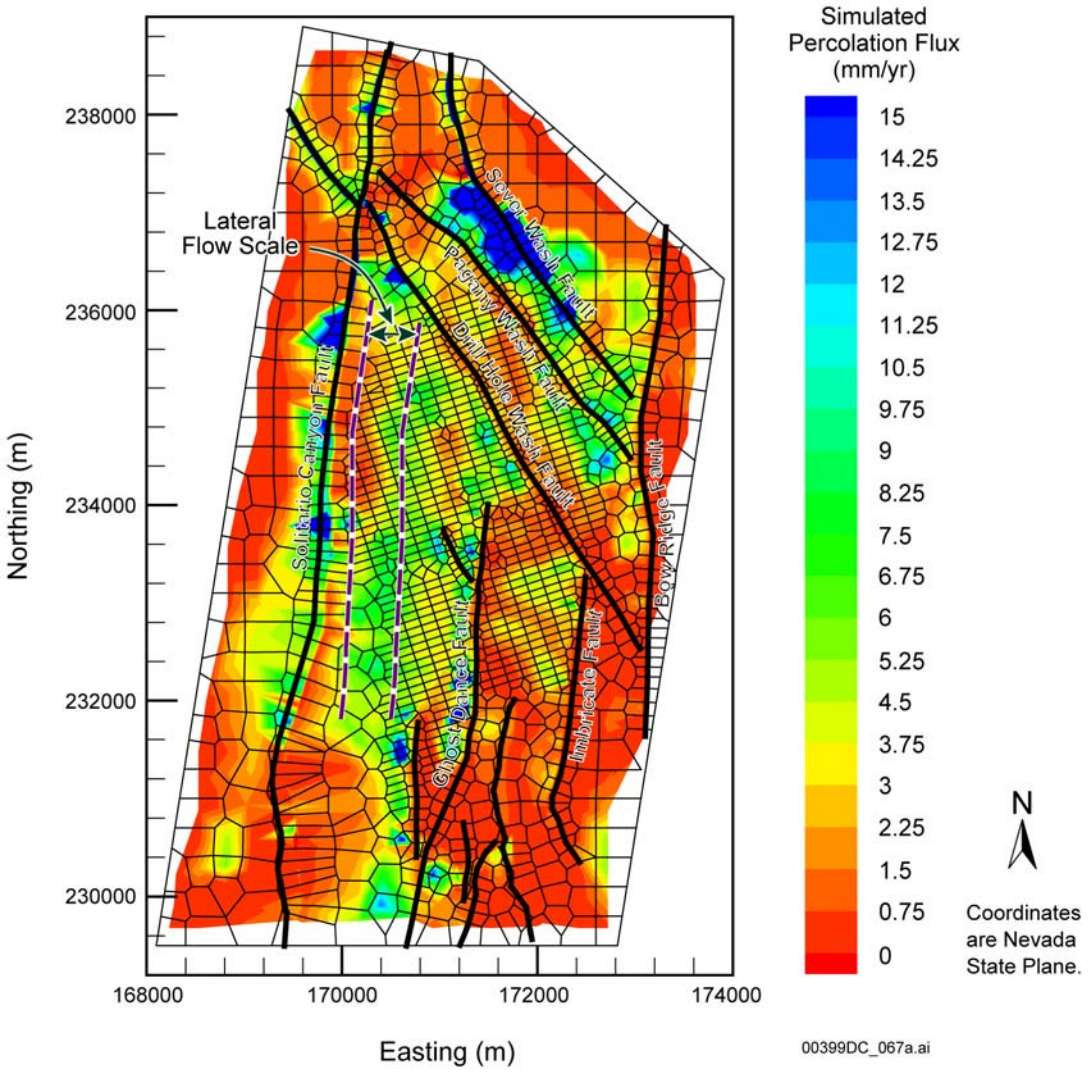

Source: BSC 2003b, Figure 6.6-1.

Figure B-3. Simulated Percolation Fluxes at the Repository Horizon under the Present-Day, Mean Infiltration Scenario, Using the Results of Simulation preq_mA

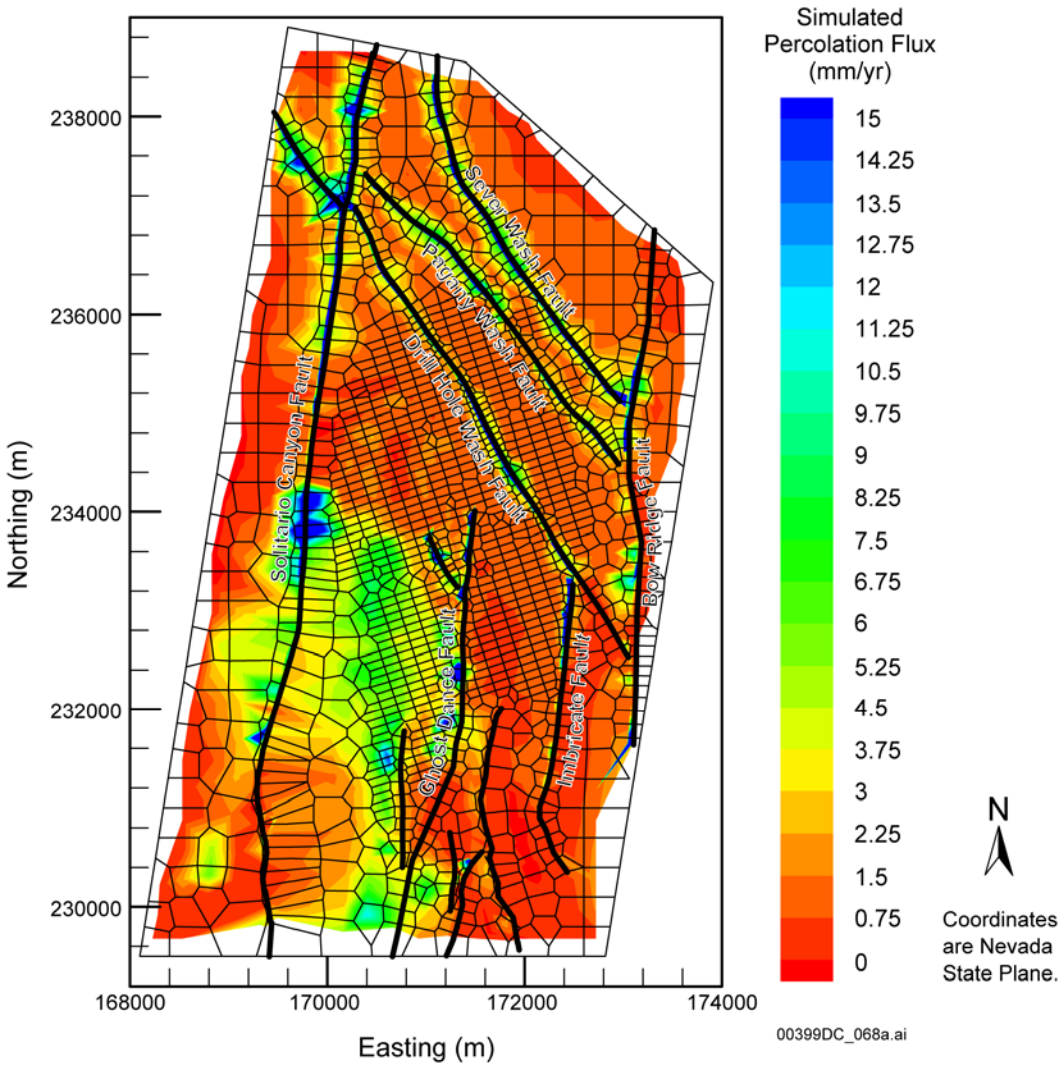

Source: BSC 2003b, Figure 6.6-6.

Figure B-4. Simulated Percolation Fluxes at the Water Table under the Present-Day, Mean Infiltration Scenario, Using the Results of Simulating the Base Case Model preq_mA

By comparing the percolation fluxes at the repository with those at the water table for the base case (e.g., Figure B-3 with Figure B-4) and the alternative case (e.g., Figure B-5 at the water table), the following findings (BSC 2003b, Section 6.6.3) are evident:

- In the northern half of the domain, the base case flow fields are very similar to the alternative ones. Because of the impact of perched water and zeolitic units, flow is mainly focused into major faults.

- In the central and southern portions of the model domain, the base case flow fields at the water table show lateral flow of several hundreds of meters to the east in the area

directly below the southern repository. This is the area where vitric zones are located within the CHn units.

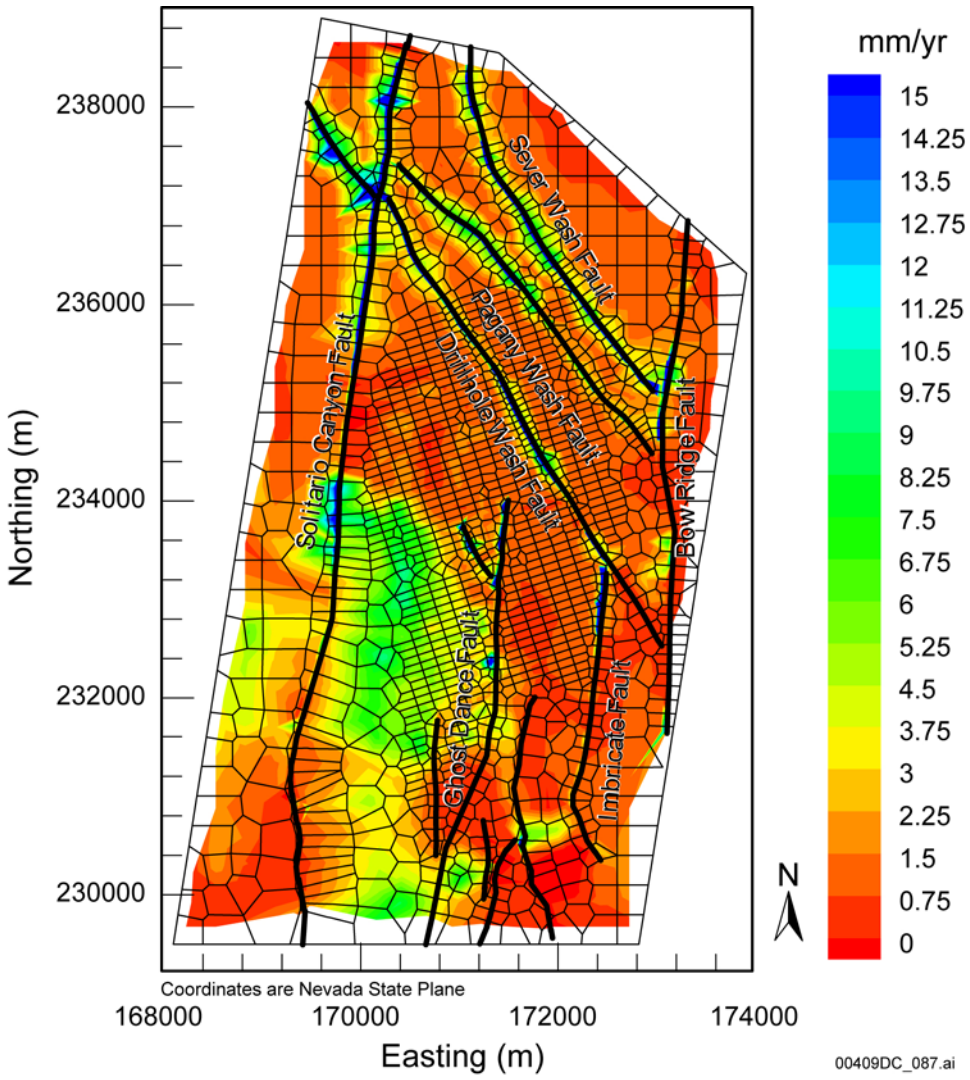

Source: BSC 2003b, Figure 6.6-7.

Figure B-5. Simulated Percolation Fluxes at the Water Table under the Present-Day, Mean Infiltration Scenario, Using the Results of Simulating the Alternative Model preq_mB

B.4.2.2 Flow Paths to the Water Table

In addition to the flux distribution discussed above (Section B.4.2.1), flow below the repository is further investigated in terms of fluxes in the matrix, fractures, and faults (BSC 2003b, Section 6.6.3). Table B-4 lists percentages of fracture–matrix flow components and fault flow at the repository horizon and the water table within the model domain. The statistics are calculated from averaging an entire layer without considering spatial distributions of flow percentage. Fracture and matrix percentages taken together produce a sum total of 100%, while fault flow percentages represent total vertical flux through fault blocks. These statistics are calculated from vertical flow along each grid column for present-day base case flow. The statistics for other

climate scenarios can be found in the *UZ Flow Models and Submodels* (BSC 2003b, Section 6.6.3).

Table B-4. Comparison of the Water Flux through Matrix, Fractures, and Faults as a Percentage of the Total Flux at the Repository and at the Water Table for the Present-Day Base Case Flow Fields

Simulation Designation	Flux at Repository Horizon (%)			Flux at Water Table (%)		
	Fracture	Matrix	Fault	Fracture	Matrix	Fault
preq_lA	91.35	8.65	58.78	78.05	21.95	71.78
preq_mA	94.29	5.71	28.62	70.29	29.71	53.73
preq_uA	94.02	5.98	27.41	77.72	22.28	60.68

Source: BSC 2003b, Table 6.6-3 (modified).
NOTE: The upper-case letter A stands for the base case model property set, the uppercase letter B for the alternative model, the lower-case letter l (before the upper case A or B) for lower bound infiltration, m for mean infiltration, and u for upper bound infiltration scenario.

These statistics indicate that fracture flow is dominant both at the repository horizon and at the water table. At the repository level, fracture flow consists of 90% to 95% of the total percolation fluxes. Fracture flow at the water table takes 70% to 80% of the total flow. On the other hand, fault flow percentage increases from about 30% at the repository to about 50% to 60% at the water table, except for the present-day, lower-bound infiltration case.

B.4.2.3 Rising Water Table

In the UZ flow model, the flow fields were calculated using a fixed water table. These flow fields can also be used for a rising-water-table case in the future. A water-rise situation can be handled by simply moving the water table up to a new elevation.

A total of six unsaturated zone flow fields for future climates (monq_lA, monq_mA, monq_uA, glaq_lA, glaq_mA, and glaq_uA) (BSC 2003b, Sections 6.6.3 and 7.11) are converted to account for a higher future water table. The six new flow fields are extracted for a rising-water-table case (BSC 2004a) in the future by vertically transecting the six flow fields with the current water table at the new water table elevation of 850 m.

Truncated steady-state unsaturated zone flow fields are expected to represent actual flow fields well. Representation of the unsaturated zone flow fields with a higher water table in the absence of direct hydrological data is justified through considering the fundamentals in model formulation (i.e., the mathematical model of the Richards equation, or more specifically, Darcy's law for description of unsaturated zone flow under a future high-water-table condition) (BSC 2004b, Sections 6.6.3 and 7.11).

The impact of a future increase in the water table is limited mainly to the lower part of the CHn units, below the repository horizon. The water table boundary is handled as a sink term in the UZ flow model. Near or at the future elevated water table, which is within the model domain of the UZ flow model, unsaturated zone flow is vertically dominant. The flow is determined primarily by the upstream or upper-layer conditions in the UZ flow model. According to

Darcy's law, in particular, the vertical flow is decided by two factors: hydraulic conductivity and hydraulic gradient. Since the vertical hydraulic gradient is dominated by a constant gravity term, and the hydraulic conductivity is upstream-weighted in the model, the change in downstream location is considered to have only a small effect on its upstream flow. Therefore, inserting a future water table boundary into the current UZ flow model will provide a good approximation for modeling the future flow fields with an elevated water table.

In addition, certain lateral flows may exist at or near a future water table, caused by intersecting perched-water, low-permeability zones. These intersected perched water or low-permeability zones will have liquid saturation near 100%, as predicted by the UZ flow model, approximately under the same conditions needed for representing a future water table boundary. Therefore, truncated flow fields at a future, higher water table, using the current unsaturated zone flow fields, will provide a reasonable representation for unsaturated zone flow fields under future climates for both vertical and lateral flow components (BSC 2004b, Section 7.11).

B.4.3 Model Calibration against Hydrological Data

The field data used in the three-dimensional UZ flow model calibration include matrix liquid saturation, matrix water-potential data, and perched-water elevations, as observed from boreholes (BSC 2003b, Section 6.2.1). Table B-5 shows the types of data from boreholes used in the calibration, and their locations are shown in Figure B-2. There is an abundance of borehole saturation data (from seven boreholes), sufficientto calibrate and validate the UZ flow model to support the flow modeling for the region below the repository in the unsaturated zone; however, there are insufficient data (from three boreholes) for water-potential measurement (Tables B-2 and B-5) (BSC 2003b, Table 6.2-1, Section 6.2.1). Moreover, the existing borehole water-potential data do not cover depths from the repository horizon to the top of CHn units. In the whole span of the repository level, the TSw units have the only available water-potential data collected locally for a few hundred meters from the entrance at the ECRB Cross Drift.

Table B-5. Borehole Data Used for Three-Dimensional Flow Model Calibration

Borehole	Matrix Liquid Saturation (core)	Matrix Liquid Water Potential	Perched-Water Elevation (masl)
USW NRG-7a	4		4
USW SD-6	4	4	
USW SD-7	4		4
USW SD-9	4		4
UE-25 SD-12	4	4	4
USW UZ-14	4		4
UE-25 UZ#16	4		
USW WT-24		4	4
USW G-2			4

Source: BSC 2003b, Table 6.2-1 (modified).

B.4.3.1 Perched Water

Perched water has been encountered in a number of boreholes at Yucca Mountain, including USW UZ-14, USW SD-7, USW SD-9, UE-25 SD-12, USW NRG-7a, USW G-2, and USW WT-24 (BSC 2003b, Table 6.2-1, Section 6.2.2.2). These perched waters occur below the repository horizon and are found to be associated with low-permeability zeolites in the CHn or the densely welded basal vitrophyre (Tptpv3, Table B-1) of the TSw units. Perched-water bodies in the vicinity of the ESF north ramp (near boreholes USW UZ-14, USW SD-9, USW NRG-7a, USW G-2, and UE-25 WT#24) are observed to occur above the base of the TSw, underlain by a zone of low-permeability zeolitized rock. The perched-water bodies in this northern area of the repository may be interconnected. However, the perched-water zones at boreholes USW SD-7 and UE-25 SD-12 are considered as local, isolated bodies.

A permeability-barrier water-perching model has been developed in the UZ flow model, in which perched waters were calibrated to match perched-water occurrences as observed at the site. Subsequently, the calibrated perched water was used to investigate the effects of flow-through and bypassing of perched bodies on tracer transport (BSC 2003b, Section 6.2).

Figure B-1 illustrates the conceptual model that characterizes potential lateral flow in the PTn units and the effects of faults and perched water on the unsaturated zone system. Perched water may occur where percolation flux exceeds the capacity of the geologic media to transmit vertical flux in the unsaturated zone. Possible mechanisms of water perching in the unsaturated zone may be permeability or capillary barrier effects at faults, or a combination of both.

In this water-perching conceptual model, both vertical and lateral water movements in the vicinity of the perched zones are considered to be controlled mainly by the fracture and matrix permeability distribution in these perched-water areas. The major aspects of the permeability-barrier conceptual model are: (1) no large-scale vertically connected potentially fluid-conducting fractures transect the underlying low-permeability units; (2) both vertical and horizontal permeabilities within and below the perched-water zone are small compared with permeabilities outside perching zones; and (3) sufficient percolation flux (greater than 1 mm/yr) exists locally. A permeability-barrier conceptual model for perched-water occurrence has been used in the UZ flow modeling studies since 1996 (Wu et al. 1999).

In the perched-water model, rock properties are locally adjusted in several grid layers of the lower basal vitrophyre in the TSw units and upper zeolites in the CHn unit. The adjustment of parameters for the modeling of perched water is detailed in the *UZ Flow Models and Submodels* (BSC 2003b, Section 6.2.3). The UZ flow model reproduces the occurrences of perched-water location well (Figures B-6 to B-8).

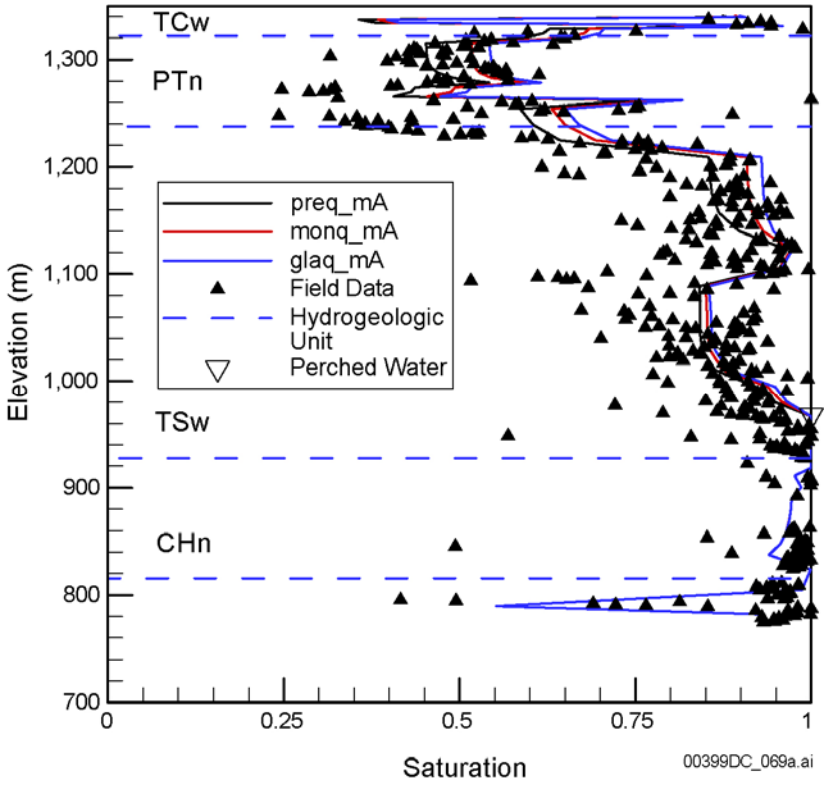

Source: BSC 2003b, Figure 6.2-2.

NOTE: The upper-case letter A stands for the base case model property set, the lower-case letter m (before the upper case letter A) for mean infiltration scenario.

Figure B-6. Comparison of Simulated and Observed Matrix Liquid Saturations and Perched-Water Elevations for Borehole USW UZ-14, Using the Results of the Simulations with Three Mean Infiltration Rates

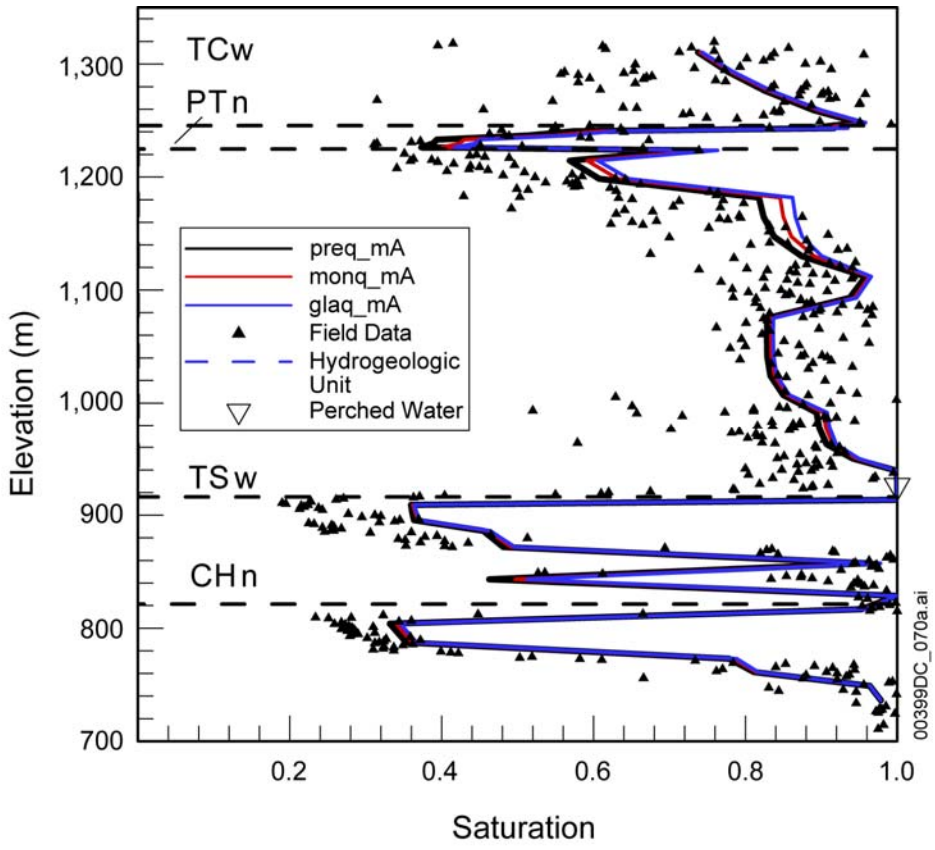

Source: BSC 2003b, Figure 6.2-3.

NOTE: The upper-case letter A stands for the base case model property set, the lower-case letter m (before the upper case A) for mean infiltration scenario.

Figure B-7. Comparison of Simulated and Observed Matrix Liquid Saturations and Perched-Water Elevations for Borehole UE-25 SD-12, Using the Results of the Simulations with Three Mean Infiltration Rates

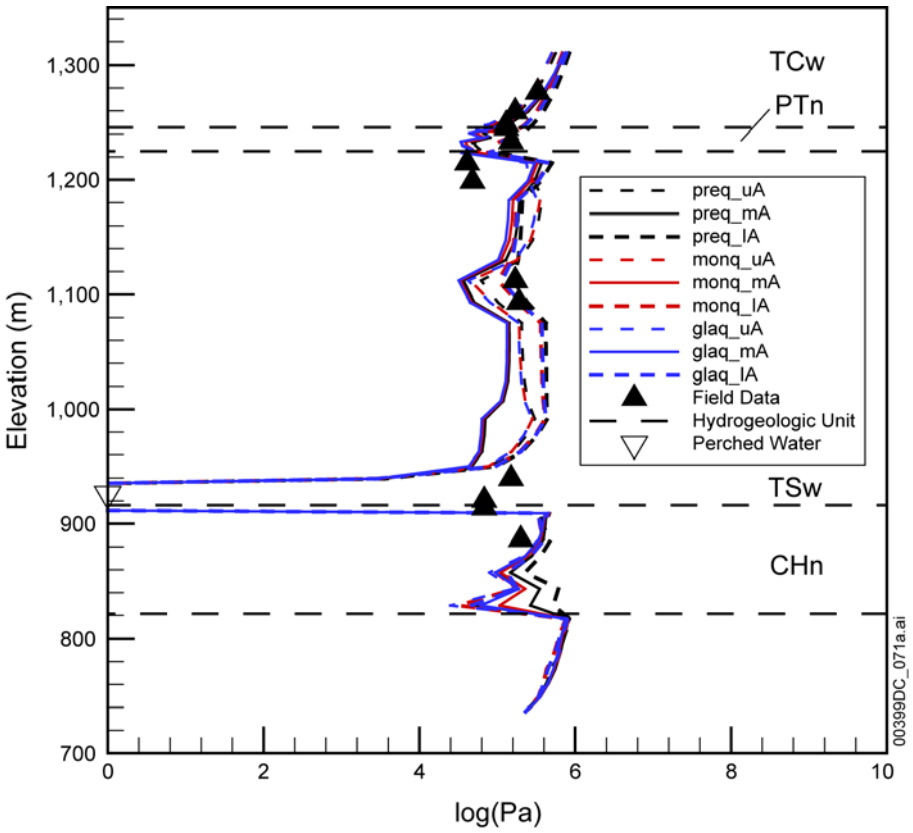

Source: BSC 2003b, Figure 6.2-4.

NOTE: The upper-case letter A stands for the base case model property set, the lower-case letter l (before the upper case A) for lower bound infiltration, m for mean infiltration, and u for upper bound infiltration scenario.

Figure B-8. Comparison of Simulated and Averaged Observed Water Potentials and Perched-Water Elevations for Borehole UE-25 SD-12, Using the Results of the Simulations with Three Mean Infiltration Rates

B.4.3.2 Matrix Saturation and Water-Potential Data

In the UZ flow model, simulations of the base-case flow models are checked against observed saturation, water potential, and perched-water data. Model results show reasonable matches with the observed hydrological data. Only a few of these comparisons are shown in the UZ flow model (BSC 2003b). Specifically, boreholes USW UZ-14 and UE-25 SD-12 are selected to show the match between observed and modeled vertical-saturation profiles and perched-water locations for simulations with perched-water occurrences (Figures B-6 to B-8).

B.4.4 Temperature Data

The analyses of temperature data provide another independent examination of percolation fluxes simulated by the UZ flow model. This is because the ambient temperature distribution within the unsaturated zone is related to percolation fluxes or infiltration rates (Bodvarsson et al. 2003). By matching borehole temperature measurements, the thermal-hydrological model helps to constrain infiltration rate ranges as well as fracture–matrix parameter values (BSC 2003b, Section 6.3.4).

Rather finely-sampled temperature profiles both above and below the repository (BSC 2003b, Table 6.3-1 and Section 7.7) were made for the three-dimensional thermal model. Specifically, qualified temperature measurements were made from the following nine boreholes:

- USW NRG-6
- USW NRG-7a
- UE-25 SD-12
- UE-25 UZ#5
- UE-25 UZ#7a
- UE-25 UZ#4
- USW H-5
- USW H-4
- UE-25 WT#18.

Boreholes UE-25 UZ#4 and UE-25 UZ#5 are so close to each other that they fall into the same grid column. Therefore, only UE-25 UZ#5 is used for calibrations. The locations of boreholes are spatially representative (Figure B-9) (BSC 2003b, Figure 6.3-1).

Figure B-10 (BSC 2003b, Figure 6.3-2) shows the final model calibrated results and measured temperature profiles in five temperature boreholes. The figure shows a good match between measured and simulated temperatures using the specified boundary conditions and the present-day, mean infiltration rate. Near the ground surface in the five boreholes, observed temperatures show significant seasonal variations. However, these seasonal changes in surface temperature have little impact on steady-state heat flow or temperature profiles in the deeper (more than 20 m) unsaturated zone.

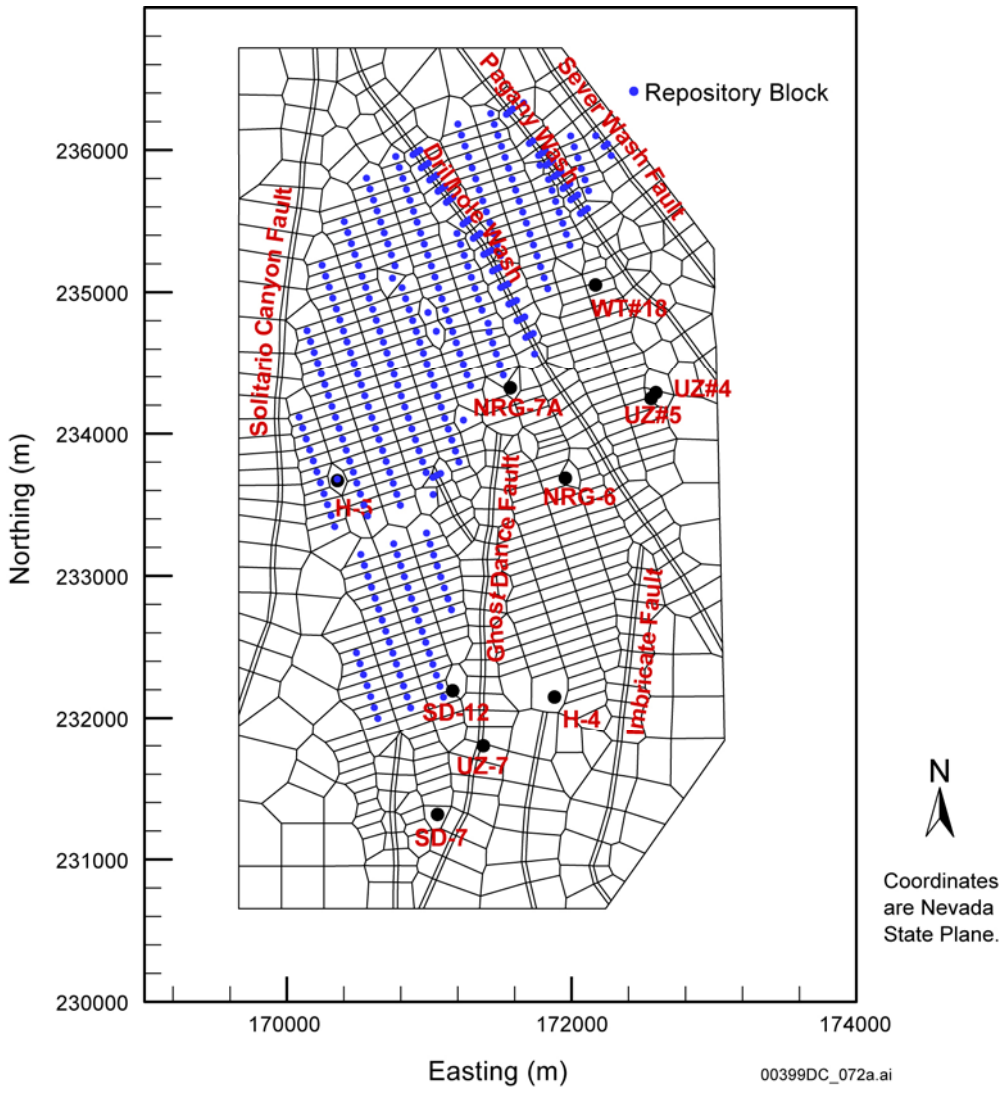

Source: BSC 2003b, Figure 6.3-1.

Figure B-9. Plan View of the Three-Dimensional Thermal Model Grid Showing the Model Domain, Faults Incorporated, Several Borehole Locations, and Thermal-Hydrological Model Boundaries

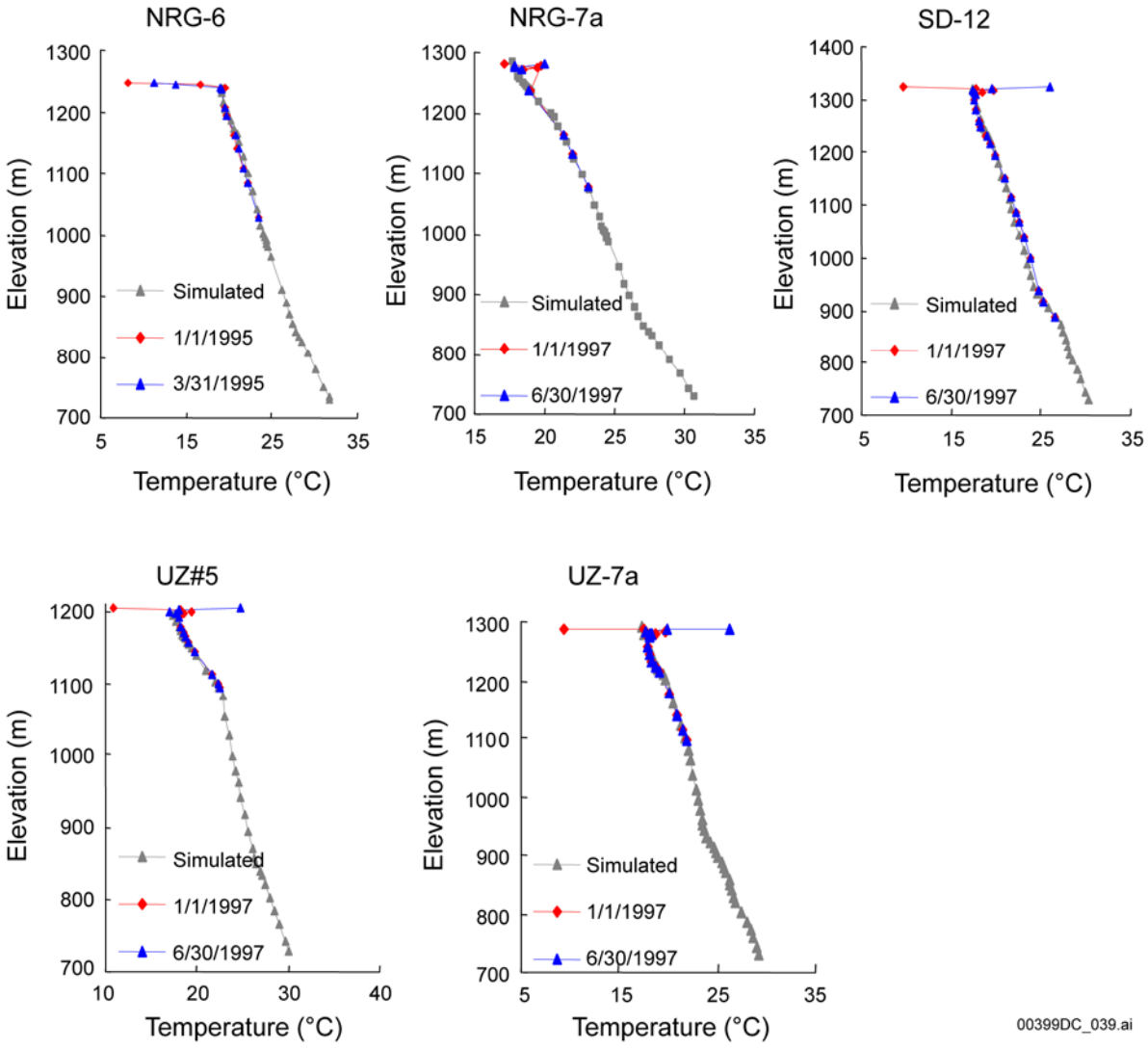

Source: BSC 2003b, Figure 6.3-2.

Figure B-10. Comparisons between Measured and Modeled Ambient Temperature Profiles for the Five Boreholes under the Present-Day Mean Infiltration Rate

In addition, the prediction of temperature is made at boreholes USW H-5, USW H-4, and UE-25 WT#18 (BSC 2003b, Section 7.7). These three boreholes penetrate the repository block and the entire unsaturated zone (see Figure B-9 for their locations) (BSC 2003b, Section 7.7). Comparisons of simulated and observed temperature profiles along these boreholes are shown in Figures B-11 to B-13, indicating a good match between the three-dimensional model prediction and observed data. Borehole USW H-5 is located close by the ECRB Cross Drift, and Figures B-11 and B-12 show that the simulated temperatures differ from observed values by less than 1.5°C in all elevations. In borehole UE-25 WT#18, the simulated results again prove to be a reasonable match with field-measured data.

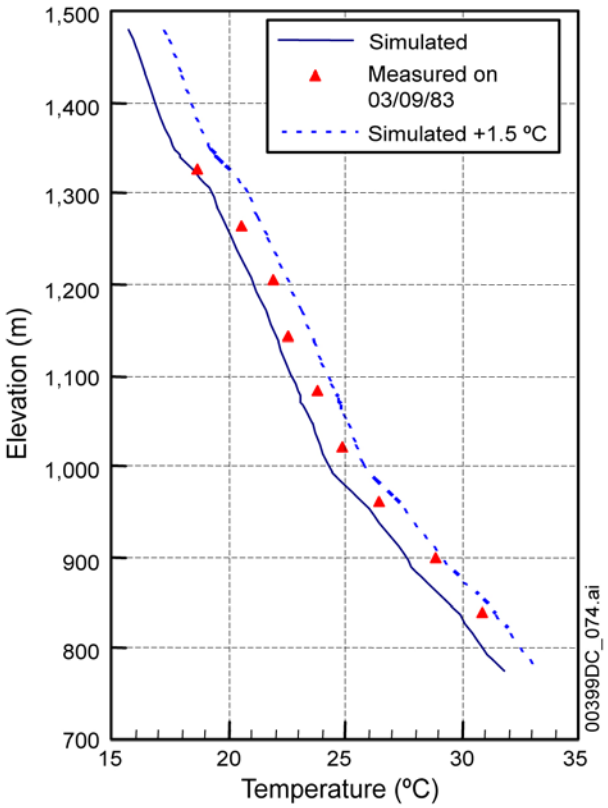

Source: BSC 2003b, Figure 7.7-1.

Figure B-11. Comparison of Simulated and Observed Temperature Profiles for Borehole USW H-5

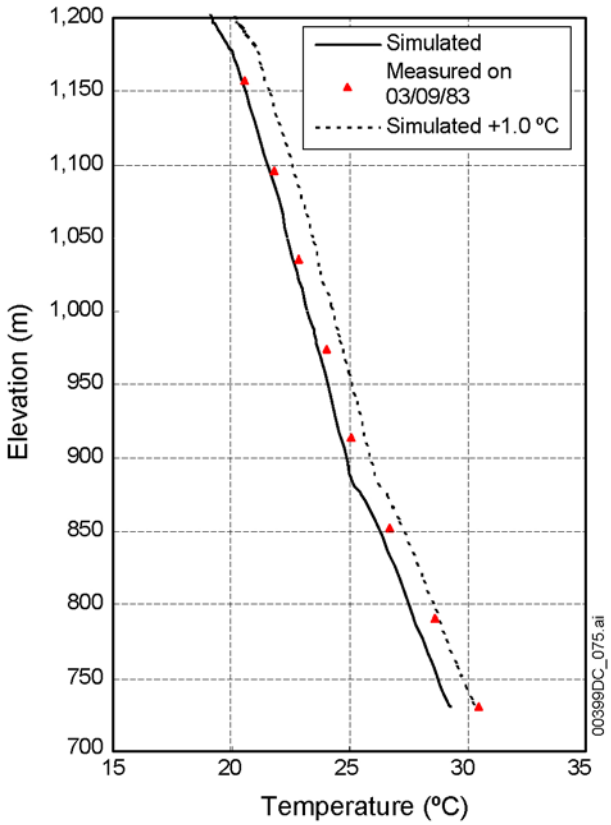

Source: BSC 2003b, Figure 7.7-2.

Figure B-12. Comparison of Simulated and Observed Temperature Profiles for Borehole USW H-4

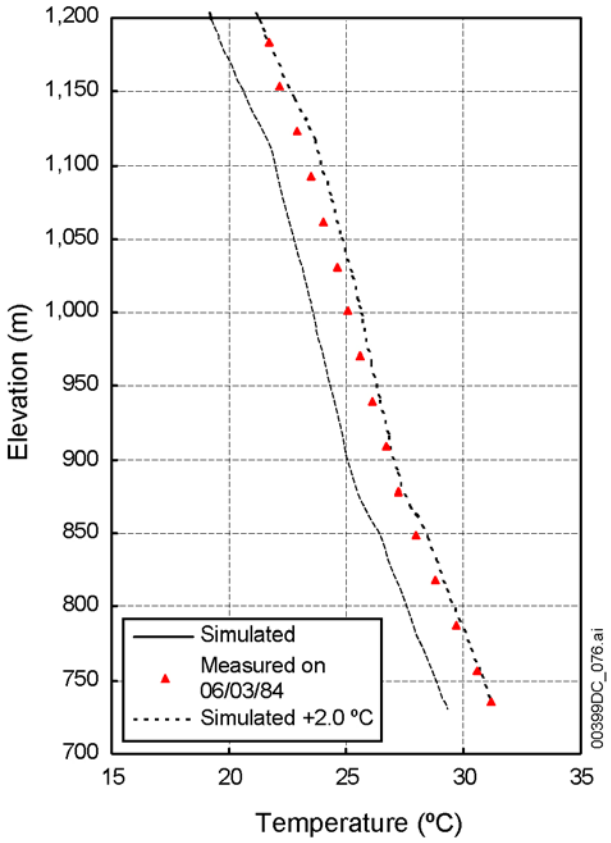

Source: BSC 2003b, Figure 7.7-3.

Figure B-13. Comparison of Simulated and Observed Temperature Profiles for Borehole UE-25 WT#18

B.4.5 Geochemical Data

Geochemical data, including chloride and strontium concentrations and calcite abundance data, were used in the calibration and validation of the UZ flow model. Available strontium concentration data are from boreholes USW SD-9 and UE-25 SD-12 and the ECRB Cross Drift (BSC 2003b, Section 7.10). Calcite data are found in boreholes USW WT-24, USW SD-6, and USW G-2 (BSC 2003b, Section 7.9). Calcite abundance data for borehole USW SD-6 were not available at the time of UZ flow modeling; modeling of calcite deposition for SD-6 was not performed (BSC 2003b, Section 7.9.5.3).

The chloride data are relatively limited at this stage, especially within the TSw and TCw units. Chloride pore-water data were collected from the ESF, ECRB Cross Drift, and 11 boreholes. However, these boreholes usually do not have data within the TSw layers. Therefore, these boreholes usually do not have data for locations around the repository level. In the ESF, chloride data are concentrated three narrow locations, with the rest of the locations blank. The chloride pore-water data for TSw layers were mainly collected from the ECRB Cross Drift and are considered locally distributed in terms of the span of the repository. Chloride data are generally limited for the CHn units.

B.4.5.1 Pore-Water Chloride Data

Chloride transport processes were also modeled in the UZ flow model analysis. The transport modeling of the conservative natural tracer chloride in the unsaturated zone is based on the conceptual model that the chloride flux as boundary input is determined from the precipitation flux and the chloride concentration in the precipitation (BSC 2003b, Section 6.5.1.2).

Chloride concentrations used in modeling were measured from pore waters extracted from field samples. These samples were collected from the ESF, the ECRB Cross Drift, and a set of eleven surface-based boreholes. The boreholes are USW SD-6, USW SD-7, USW SD-9, UE-25 SD-12, USW NRG-6, USW NRG-7a, USW UZ-14, UE-25 UZ#16, UE-25 UZ#7a, USW WT-24, and USW G-2 (BSC 2003b, Table 6.5-1 Section 6.5) (see Figure B-2 for their locations).

Even with all the various sources for pore-water chloride data, limitations on this data exist. Generally, boreholes do not have pore-water data from the TSw and TCw units, and rarely have an evenly distributed or complete data profile. Most of the chloride data of the TSw units were sampled from the ECRB Cross Drift. Early chloride data collected from the ECRB Cross Drift were available for the 2001 UZ flow model (BSC 2001b). Another set of chloride (of another composition) data was recently collected from the ECRB Cross Drift, which was not available at the time of the 2003 UZ flow model (BSC 2003b). However, these latest ECRB chloride data are considered to be redundant in some sense, because they were from a repeated sampling over the region that had been covered by the previously available chloride data. The amount of the ESF chloride data is small and has limited spatial representation. The available data are restricted to three local segments (located in 700-1,100 m, 3,600-3,700 m, and 6,600-7,500 m from the north portal entrance). Generally, the 11 boreholes do not data covering the TSw and TCw layers. Boreholes USW NRG-6 and UE-25 UZ#7a have no chloride below the repository at all. The limited data for the TSw and TCw welded tuff units historically result from the difficulty in obtaining enough pore waters for chemical analysis (owing to the low water content in the nonwelded tuffs).

For the CHn layers below the repository, chloride data were unevenly distributed, and most of those boreholes that have some chloride data in the CHn layers usually do not have any chloride data in other layers.

Figures B-14 and B–15 show the results of chloride modeling in boreholes USW NRG-6 and USW UZ-14 (BSC 2003b, Table 6.5.2, Section 6.5.1.2). These figures plot the chloride profiles of present-day infiltration rates of mean infiltration with lower and upper bounds. The results demonstrate that the mean infiltration case has the closest match between the calculated concentrations and the field-measured chloride data. The upper-bound case shows a moderate match; the lower-bound case shows the least match.

A comparison between the base-case model and the alternative model results for borehole USW SD-9 is plotted in Figure B-16, and that for the ECRB Cross Drift is in Figure B-17 and Table B-6. In base case A, the UZ flow model uses the property set for the PTn that would favor lateral diversion of flow. In the alternative model B, the UZ flow model uses a different property set for the PTn, one that does not favor large-scale lateral diversion (BSC 2003b, Table 6.5-2).

Comparative studies of chloride distributions, simulated using the base case and alternative flow fields, indicate generally that the base case flow field simulation results provide an overall better match with the observed chloride. Statistics of the ECRB profile shows that the base-case models consistently yield closer matches than the alternative models for all the infiltration scenarios (Table B-6). The ECRB is considered to be susceptible to the effect of the flow pattern at the PTn units, because it runs transverse the Mountain ridge, and is located right below the PTn units. The main difference between the base-case and alternative flow fields is whether there is large- or small-scale lateral flow within the PTn units, while the base-case flow fields predict relatively large lateral diversion in general (BSC 2003b, Sections 6.2.5 and 6.6.3). Model calibration results with chloride data further reveal that large lateral diversion may exist in the PTn units. Therefore, pore-water chloride may provide key evidence for understanding flow pattern in the PTn units, which has had a direct impact on chloride transport and distributions (BSC 2003b, Section 6.5.2.2).

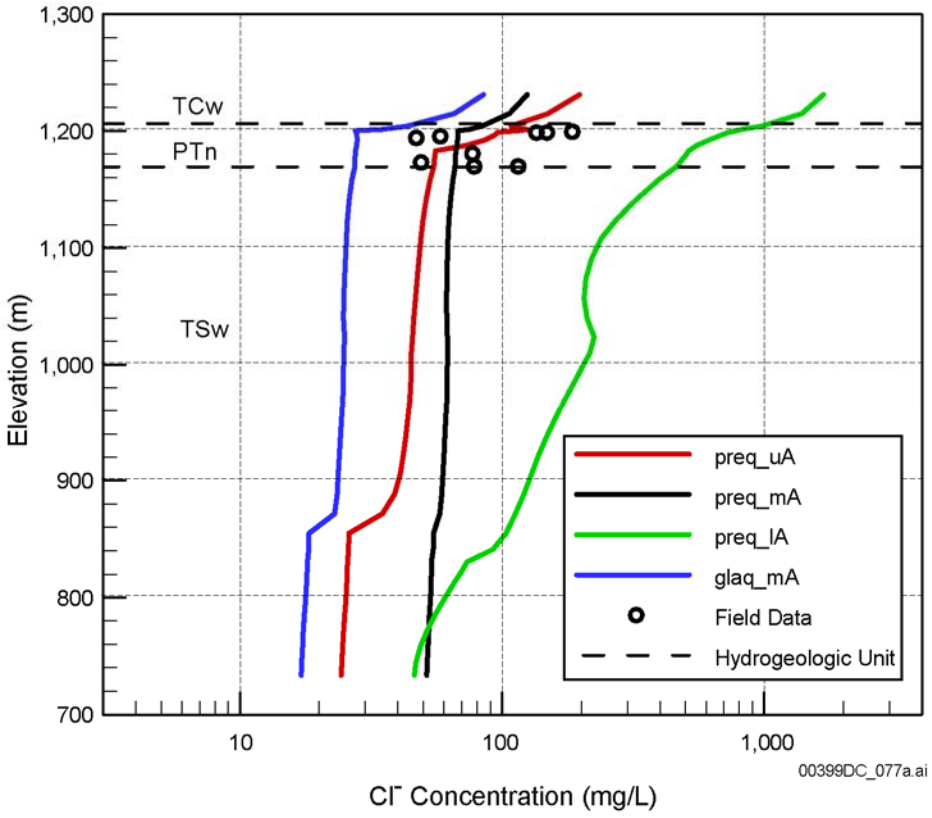

Source: BSC 2003b, Figure 6.5-1.

NOTE: The upper-case letter A stands for the base case model property set, the lower-case letter l (before the upper case A) for lower bound infiltration, m for mean infiltration, and u for upper bound infiltration scenario.

Figure B-14. Chloride Concentration Profiles at Borehole USW NRG-6 for Present Recharge (with Mean, Upper, and Lower Bounds) and Glacial Recharge

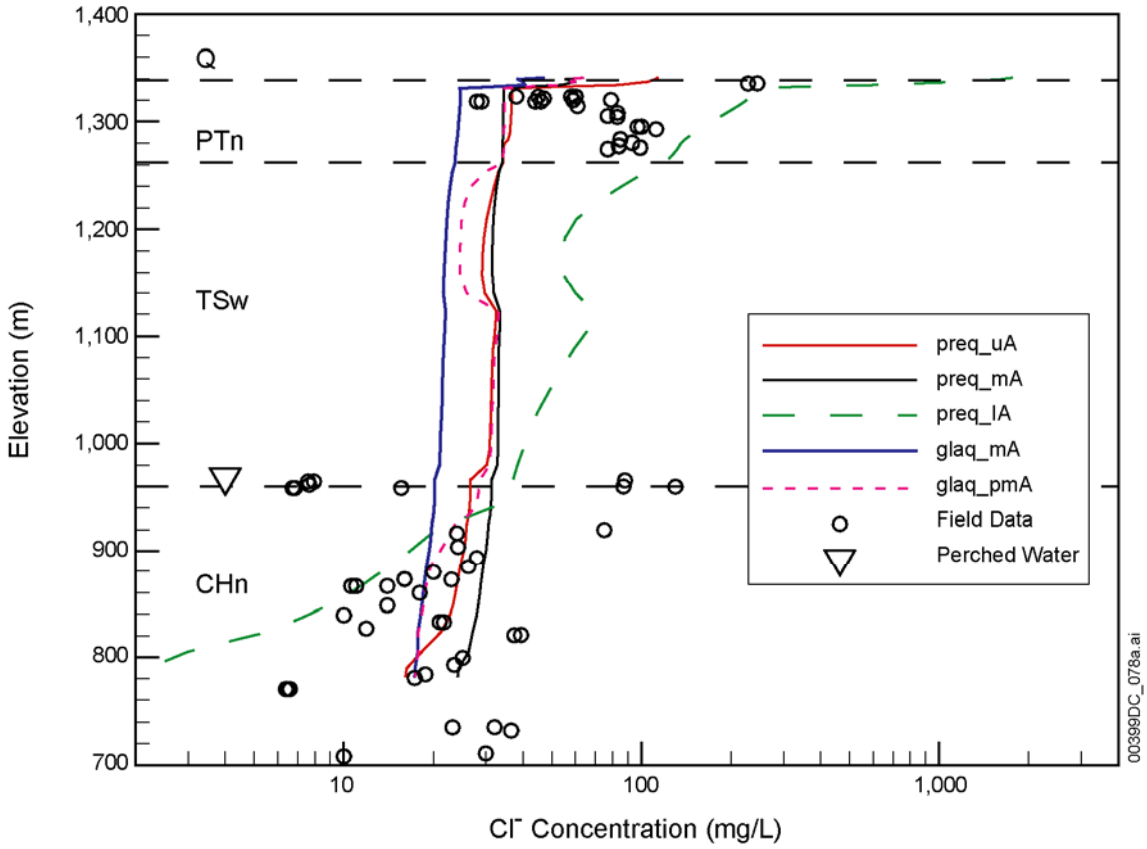

Source: BSC 2003b, Figure 6.5-2.

NOTE: The upper-case letter A stands for the base case model property set, the lower-case letter l (before the upper case A) for lower bound infiltration, m for mean infiltration, and u for upper bound infiltration scenario.

Figure B-15. Chloride Concentration Profiles at Borehole USW UZ-14 for Present Recharge (with Mean, Upper, and Lower Bounds) and Glacial Recharges

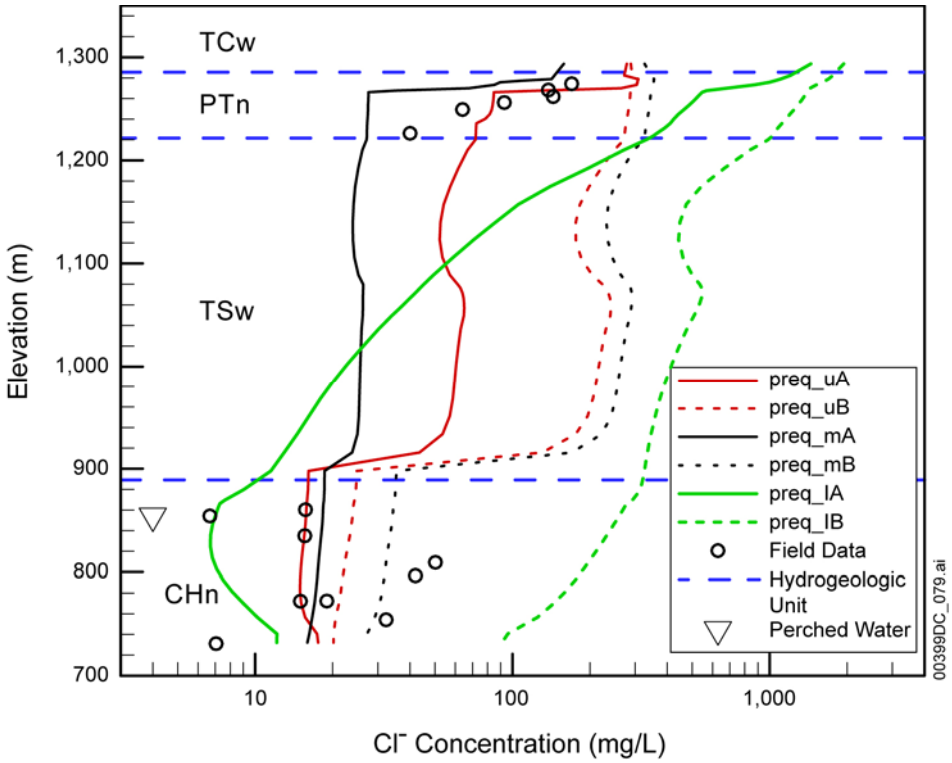

Source: BSC 2003b, Figure 6.5-3.

NOTE: The upper-case letter A stands for the base case model property set, the uppercase letter B for the alternative model, the lower-case letter l (before the upper case A or B) for lower bound infiltration, m for mean infiltration, and u for upper bound infiltration scenario.

Figure B-16. Chloride Concentration Profiles at Borehole USW SD-9 for Present Recharge (with Mean, Upper, and Lower Bounds) and Glacial Recharge

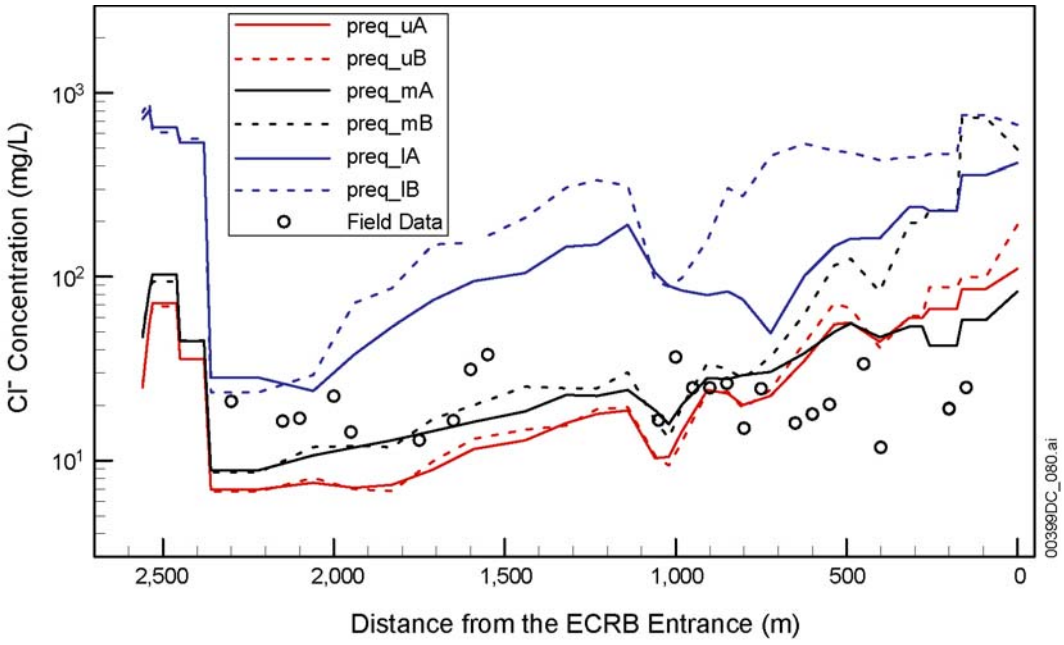

Source: BSC 2003b, Figure 6.5-4.

NOTE: The upper-case letter A stands for the base case model property set, the upper-case letter B for the alternative model, the lower-case letter l (before the upper case A or B) for lower bound infiltration, m for mean infiltration, and u for upper bound infiltration scenario.

Figure B-17. Chloride Concentration Profiles at the ECRB Cross Drift for Present Recharge with Mean, Upper, and Lower Bounds

Table B-6. Comparison of Simulated Pore Water Chloride Concentrations with Measured Chloride Concentrations at the ECRB

RMS†	Lower Bound Infiltration	Mean Infiltration	Upper Bound Infiltration
Base Case Model (A)	120.0	18.0	24.5
Alternative Model (B)	340.8	183.6	31.4

Source: Measured chloride data from DTN LA0002JF12213U.002; Cl transport simulation results from BSC 2003b (Figure 6.5-4) and DTN LB0303CLINFL3D.001.

Note: †root mean square (RMS) of calculated concentrations with gridblock averaged measured concentrations. $\mathrm{RMS} = [\frac{1}{n-1}\sum_{i=1}^{n}(c-\overline{o})^2]^{1/2}$, where c is the simulated concentrations and $\overline{o}$ is the gridblock-averaged measured concentration, n is the number of concentration data (gridblock averaged) in the RMS calculation (n = 18).

B.4.5.2 Strontium Concentrations

The modeling of strontium in the unsaturated zone assumes that the infiltration at the surface is the only source of strontium input (BSC 2003b, Section 7.10). Strontium data are measured values for pore salts extracted (by leaching) from surface-based boreholes USW SD-9 and UE-25 SD-12, as well as from perched waters and pore waters obtained by ultracentrifugation of core samples from the ECRB Cross Drift (BSC 2003b, Section 7.10.3).

In Figure B-18, modeled strontium concentrations are compared to these measured values for boreholes SD-9 and SD-12. Modeling results are shown to match the observed data well. Measured concentrations in the unsaturated zone above the perched water show a range of concentrations from about 0.1 to 2 mg/L, with perched-water concentrations (and pore-water concentrations at a similar depth) closer to 0.01 mg/L. This sharp reduction in strontium concentrations is greater than the equivalent drop in chloride concentrations in the perched-water bodies and is consistent with ion exchange in zeolitic rocks. The steady-state modeled concentrations above the perched water are very close to the mean values in boreholes USW SD-9 and UE-25 SD-12. Where perched-water samples were collected in USW SD-9, the model results capture the drop in concentration quite closely. In UE-25 SD-12, the measured and modeled concentrations below 900 m exhibit a reversal to higher concentrations. This reversal is consistent with lateral flow in the vitric units, rather than simple vertical flow through the zeolitic units that would result in consistently low concentrations below them.

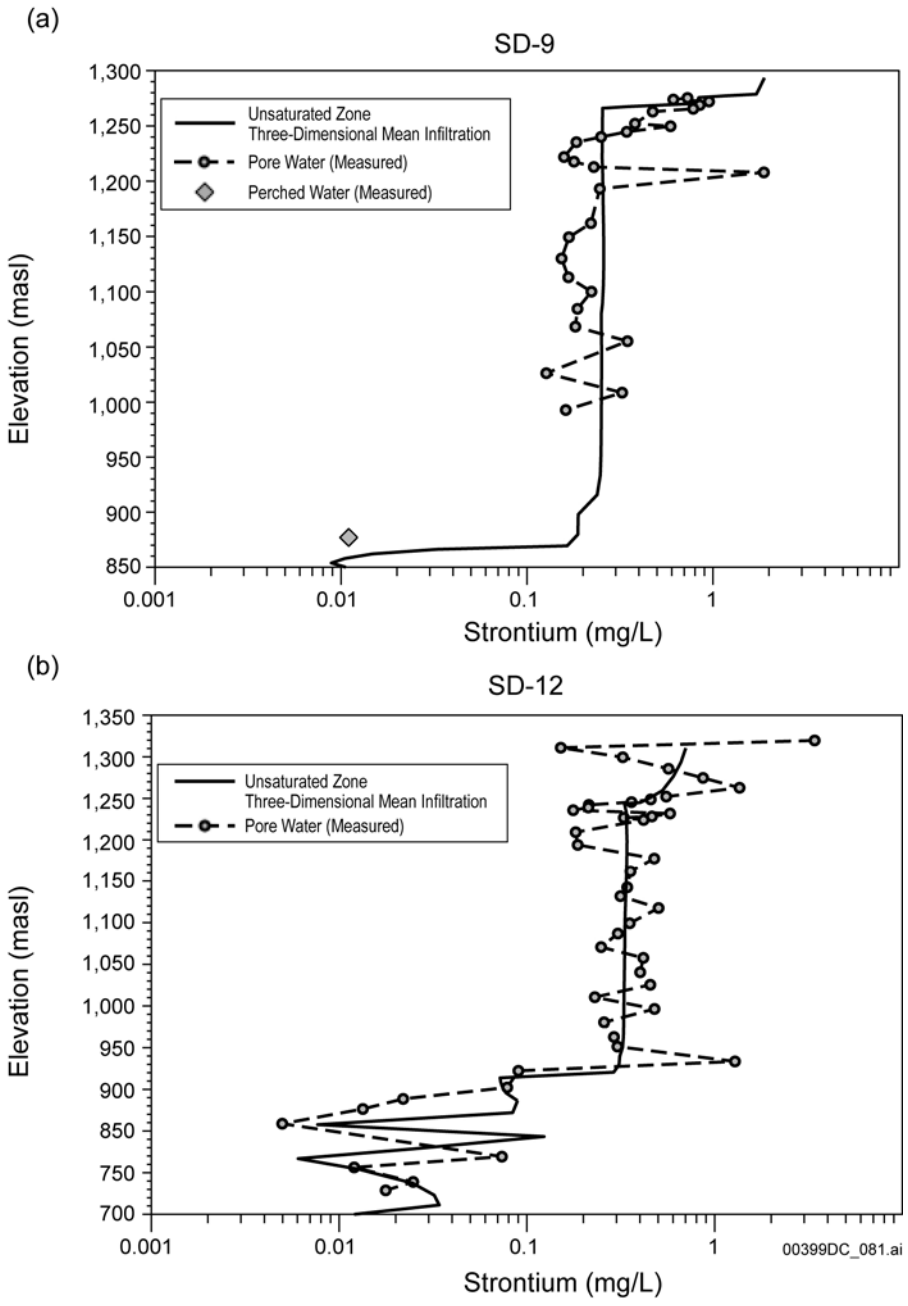

Source: BSC 2003b, Figure 7.10-1.

Figure B-18. Comparison of Measured and Modeled Strontium Concentrations as a Function of Elevation for the Surface-Based Boreholes (a) USW SD-9 and (b) UE-25 SD-12

B.4.5.3 Calcite Modeling

Analyses of precipitated calcite data in the unsaturated zone also provide information to constrain the infiltration flux. The calcium concentration and CO_2 partial pressure in percolating water are the major factors controlling the abundances of calcite and its stability. The primary driving force for calcite precipitation from percolating waters in the unsaturated zone is its

decreasing solubility with increasing temperature; calcite precipitates as water flows downward because of the geothermal gradient (BSC 2003b, Section 7.9.2).

One-dimensional modeling was performed for calcite deposition. Results were compared mainly with available measured calcite abundance from a deep borehole (UE-25 WT-24), with referencing to calcite data from USW SD-6 and USW G-2 (BSC 2003b, Section 7.9). Simulations were performed using three infiltration rates, a base case rate of 5.92 mm/yr (BSC 2003d), and bounding rates of 2 mm/yr and 20 mm/yr. Over a range of 2 to 20 mm/yr infiltration rates, the simulated calcite abundances generally fall within the range of calcite observed in the field (Figure B-19) (BSC 2003b, Section 7.9.5.1, Figure 7.9-3), which satisfies the validation criterion. The modeled calcite abundances generally increase with increasing infiltration rate (BSC 2003b, Section 7.9.6). Figure B-19 represents simulation results from a comprehensive geochemical system that considers pH effect, CO_2 partial pressure, a broad assemblage of minerals (including all aluminosilicates, as well as Fe- and Mg-bearing minerals), and aqueous species (BSC 2003b, Section 7.9.4.2, Table 7.9-2). The 20 mm/yr infiltration rate may be the upper bound for UE-25 WT-24 location, whereas the base case infiltration rate (5.92 mm/yr) used for the flow model gives the closest match to the data (BSC 2003b, Section 7.9.6). Modeling calcite deposition provides additional evidence for validation of the UZ flow model.

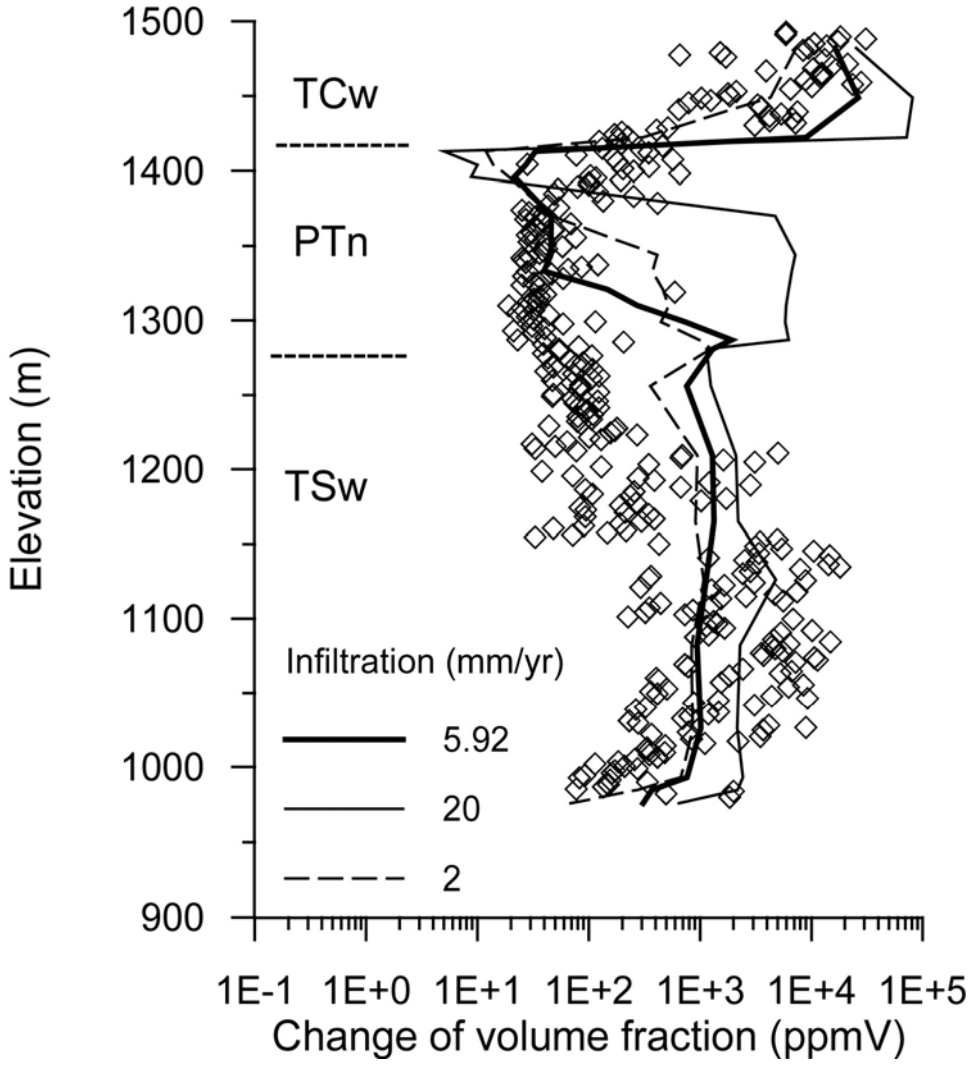

Source: BSC 2003b, Figure 7.9-3a.

Figure B-19. Simulated Total (Fracture plus Matrix) Calcite Abundances (in Part per Million Volume (ppmV) or 10^{-6} Volume Fraction) in Borehole WT-24 for Different Infiltration Rates after 10 Million Years

B.4.6 Compositions of Infiltration Waters in the Thermal-Hydrological-Chemical Model

The amount of available data for infiltrating water has increased significantly since GEN 1.01 (Comment 106) was made. In the initial 2000 version of *Drift-Scale Coupled Processes (DST and THC Seepage) Models* (BSC 2003c, Section 6.2.2.1), the available data on infiltrating waters comprised three samples of one type of water (the HD-PERM samples), ultracentrifuged from core samples collected from the Tptpmn geologic unit in Alcove 5 near the Drift Scale Test. By the time of the 2003 revision of the *Drift-Scale Coupled Processes (DST and THC Seepage) Models* (BSC 2003c), a series of pore-water samples had been collected (BSC 2003c,

Section 6.2.2.1) from the following repository host units: the upper lithophysal zone (Tptpul), middle nonlithophysal zone (Tptpmn), and lower lithophysal zone (Tptpll). These samples were ultracentrifuged from core collected in the ECRB Cross Drift and in boreholes USW UZ-14, USW SD-9 and USW NRG-7/7a (a total of 5 borehole pore-water samples from the TSw units). The compositions of these waters are shown on a Piper diagram in Figure B-20. For comparison, the figure also plots other water compositions, including perched water and pore water at similar depths (base of Tptpln) in borehole USW UZ-14, and groundwater from well J-13.

Possible choices of potential initial water compositions for the thermal-hydrological-chemical seepage model span a wide range, with HD-PERM samples at one end (calcium-sulfate-chloride type) and groundwater from well J-13 at the other end (sodium-bicarbonate type) (Figure B-20).

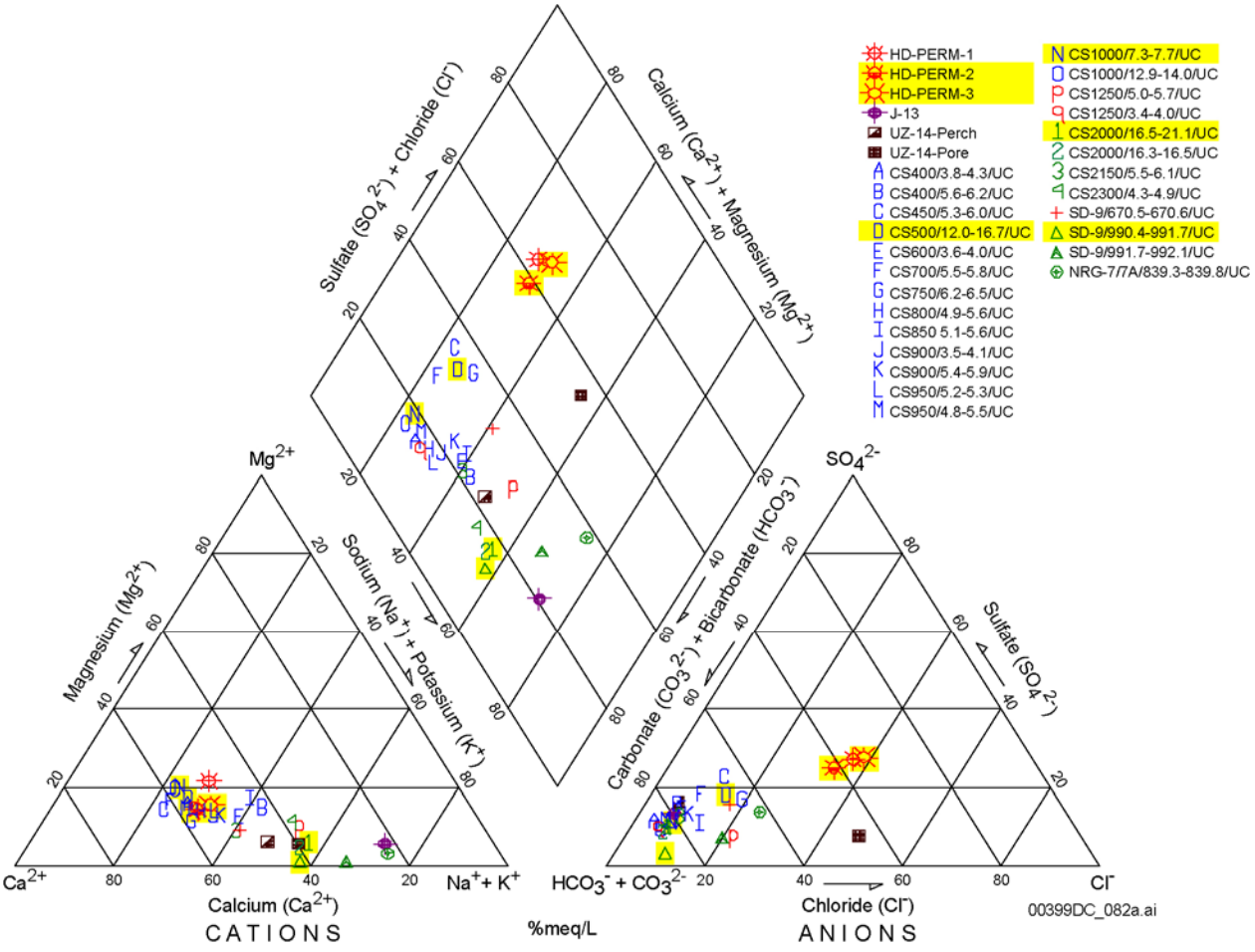

Source: BSC 2003c, Figure 6.2-4.

NOTE: Samples labeled HD-PERM are pore waters from the Tptpmn unit in Alcove 5 of the ESF. Samples IDs starting with CS represent pore waters from ECRB Cross Drift and are listed in order of increasing distance (m) into the drift (down stratigraphy), with labels reflecting lithostratigraphic units as follows: Tptpul (capitals A-O), Tptpmn (lower case p-q), and Tptpll (numbers 1-4). Additional borehole interval information after each CS sample labeling is sample interval distances from borehole collar given in feet. CS is abbreviation for Construction Station, indicating distance along the ECRB Cross Drift in meters. Sample IDs starting with USW SD-9 and USW NRG-7 represent pore waters from boreholes with the same names and show the sampling interval in feet from ground surface. The first USW SD-9 sample at 670 ft is from the base of the

Tptpul, and the others are from the Tptpll. The USW NRG-7 sample is from the Tptpmn. Yellow-highlighted samples are those selected water types (W0 as ☼; W4 1; W5 N; W6 ∆; and W7 D; see following text).

Figure B-20. Piper Plot of Water Compositions from Repository Units

The following water compositions were selected, listed here with an assigned arbitrary identification (W0, W5, etc.), for the thermal-hydrological-chemical seepage model:

W0: HD-PERM water, from the Tptpmn unit in Alcove 5.

W4: Sample CS-2000/16.5-21.1/UC, from the Tptpll lithostratigraphic unit in the ECRB Cross Drift.

W5: Sample CS-1000/7.3-7.7/UC, from the base of the Tptpul lithostratigraphic unit in the ECRB Cross Drift.

W6: Sample SD-9/990.4-991.7, from the Tptpll lithostratigraphic unit in borehole USW SD-9.

W7: Sample CS500/12.0-16.7, from the Tptpul lithostratigraphic unit in the ECRB Cross Drift.

These five samples cover a significant portion of the spectrum of water types, and yet differ from one another in significant ways (Figure B-20). Water types W0, W4 (or W6), and W5 occupy the higher ends of sulfate/chloride, calcium/magnesium, and sodium/potassium, respectively. W0 (the HD-PERM samples) plots higher than other pore waters on the diamond-shaped area in Figure B-20, bounding the range of compositions in the calcium-sulfate-chloride field.

W4 and W6 exhibit the lowest (Ca+Mg)/(Na+K) ratio of the ECRB Cross Drift samples. W4 also contains a higher fluoride concentration than the other samples and exhibits better charge balance than other samples of similar composition. W6 contains a higher nitrate concentration compared to most other samples and exhibits a better charge balance than W4. The W7 sample plots between Water W0 (the HD-PERM waters) and Water W5 on Figure B-20, further capturing the variability of water compositions in the upper part of the figure.

These five types of waters were chosen, with preference given to actual pore waters from unsaturated regions within or above the repository units and exclusion of waters from perched water zone and saturated zone (BSC 2003c, Section 6.2.2.1). This is based on a number of considerations. The perched waters below the repository are generally much more dilute than unsaturated zone pore waters because isotopic compositions ($^{36}Cl/Cl$, $^{18}O/^{16}O$, D/H, ^{14}C) and chloride concentrations suggest that the perched waters have a large proportion of late Pleistocene-early Holocene water (Levy et al. 1997, p. 906; Sonnenthal and Bodvarsson 1999, pp. 107 and 108). The saturated zone water is also more dilute than pore waters, and neither saturated nor perched water reflect calculated CO_2 partial pressures consistent with CO_2 concentrations in gas measured in the unsaturated zone in repository units. The saturated zone and perched-water compositions are therefore deemed poor candidates as initial-input water compositions for the thermal-hydrological-chemical seepage model.

The choice of input water composition also must take into account the natural variability of pore-water compositions in the repository units, as illustrated in Figure B-20. However, because these samples were mainly from the ECRB Cross Drift, the spatial coverage of these data is too small to derive a probability of occurrence for any of these pore-water compositions.

The differences in the proportions (not absolute values) of cations and anions in analyzed waters have an important bearing on the types of residual brines that could develop upon evaporation and boiling due to thermal loading (BSC 2003h). Should these waters seep onto the surface of a hot waste package, knowledge of their end-brine composition is important to assess the likelihood and intensity of waste package corrosion (BSC 2004c). Therefore, the span of selected input water compositions could be used to check whether the selection has taken into account factors that influence the end-brine composition of these waters.

Evaporation can turn dilute groundwater into corrosive brine, and complete evaporation can result in the precipitation of hygroscopic salts (which have the ability of different brines or salts to absorb water from the air). Among the concerns is the formation of potentially deleterious brines such as calcium (and magnesium) chloride rather than sodium chloride, or brines that are less hygroscopic. Factors such as composition plotting in the upper half of the diamond-shaped area of Figure B-20, together with low nitrate and sulfate concentrations relative to chloride, could be used to infer a higher likelihood of potentially deleterious brines developing.

As water evaporates from solution, dissolved solids concentrate until they become supersaturated with respect to a solid phase. If a solid phase is a binary salt, and the normalities of the two reactants are not equal, the reactant having the lower normality will become depleted in solutions, while the reactant with higher normality will continue to concentrate. This mechanism is known as chemical divide. (Even if the normalities are close to each other, they will evolve quickly to differentiate themselves.)

Calcium chloride brines are more likely to form after calcite precipitation chemical divide if the total calcium concentration (in meq/L) exceeds the total aqueous carbonate concentration (in meq/L) in the initial water. Waters with such compositions would have a tendency to plot in the upper half of the diamond-shaped area in Figure B-20, although other waters may also plot in this area if their magnesium concentration were high relative to calcium. Other less hygroscopic salts are most likely formed from original waters if the nitrate and sulfate concentration in the original solution were elevated relative to chloride.

In summary, five types of infiltrating waters were chosen from the pore waters at or above the repository horizon. The samples were mainly from the ECRB Cross Drift, and thus do not have sufficient spatial variation to warrant a probability analysis of their occurrences. J-13 water and UZ-14 pore water, although seemingly end-members of waters from the Yucca Mountain and the vicinity, were not included in the selections, because their compositions contrasted with the pore waters in the repository horizon. However, this end-member type of water with very low chloride concentrations in the ESF pore waters, likely has occurred in the ESF pore waters. A recent study showed that pore waters with low chloride concentrations were found in the ESF. These chloride concentrations were estimated to be as low as that of the J-13 well water (Lu et al. 2003, Section 4.4). The waters with very low chloride concentration were related to fracture or fault zones where bomb-pulse ^{36}Cl was found (Gascoyne 2003, p. 343). Overall,

given the limitations in available data, the five infiltrating waters represent a reasonably approximate selection of water samples plotted in Figure B-20.

B.5 REFERENCES

Bodvarsson, G.S.; Kwicklis, E.; Shan, C.; and Wu, Y.S. 2003. "Estimation of Percolation Flux from Borehole Temperature Data at Yucca Mountain, Nevada." *Journal of Contaminant Hydrology*, 62–63, 3–22. New York, New York: Elsevier. TIC: 254205.

BSC (Bechtel SAIC Company) 2001a. *FY 01 Supplemental Science and Performance Analyses, Volume 1: Scientific Bases and Analyses*. TDR-MGR-MD-000007 REV 00 ICN 01. Las Vegas, Nevada: Bechtel SAIC Company. ACC: MOL.20010801.0404; MOL.20010712.0062; MOL.20010815.0001.

BSC 2001b. *UZ Flow Models and Submodels*. MDL-NBS-HS-000006 REV 00 ICN 01. Las Vegas, Nevada: Bechtel SAIC Company. ACC: MOL.20020417.0382.

BSC 2002. *Geologic Framework Model (GFM2000)*. MDL-NBS-GS-000002 REV 01. Las Vegas, Nevada: Bechtel SAIC Company. ACC: MOL.20020530.0078.

BSC 2003a. *Radionuclide Transport Models Under Ambient Conditions*. MDL-NBS-HS-000008 REV 01. Las Vegas, Nevada: Bechtel SAIC Company. ACC: DOC.20031201.0002.

BSC 2003b. *UZ Flow Models and Submodels*. MDL-NBS-HS-000006 REV 01. Las Vegas, Nevada: Bechtel SAIC Company. ACC: DOC.20030818.0002.

BSC 2003c. *Drift-Scale Coupled Processes (DST and THC Seepage) Models*. MDL-NBS-HS-000001 REV 02. Las Vegas, Nevada: Bechtel SAIC Company. ACC: DOC.20030804.0004.

BSC 2003d. *Calibrated Properties Model*. MDL-NBS-HS-000003 REV 01. Las Vegas, Nevada: Bechtel SAIC Company. ACC: DOC.20030219.0001.

BSC 2003e. *Development of Numerical Grids for UZ Flow and Transport Modeling*. ANL-NBS-HS-000015 REV 01. Las Vegas, Nevada: Bechtel SAIC Company. ACC: DOC.20030404.0005.

BSC 2003f. *In Situ Field Testing of Processes*. ANL-NBS-HS-000005 REV 02. Las Vegas, Nevada: Bechtel SAIC Company. ACC: DOC.20031208.0001.

BSC 2003g. *Mountain-Scale Coupled Processes (TH/THC/THM)*. MDL-NBS-HS-000007 REV 01. Las Vegas, Nevada: Bechtel SAIC Company. ACC: DOC.20031216.0003.

BSC 2003h. *In-Drift Precipitates/Salts Model*. ANL-EBS-MD-000045 REV 01 ICN 01B. Las Vegas, Nevada: Bechtel SAIC Company. ACC: DOC.20031028.0003.

BSC 2004a. *Particle Tracking Model and Abstraction of Transport Processes*. MDL-NBS-HS-000020 REV 00. Las Vegas, Nevada: Bechtel SAIC Company. ACC: DOC.20040120.0001.

BSC 2004b. *UZ Flow Models and Submodels*. MDL-NBS-HS-000006 REV 01 ICN 01A. Las Vegas, Nevada: Bechtel SAIC Company. ACC: MOL.20040126.0082.

BSC 2004c. *Engineered Barrier System: Physical and Chemical Environment Model*. ANL-EBS-MD-000033 REV 02. Las Vegas, Nevada: Bechtel SAIC Company. ACC: DOC.20040212.0004.

Cornell, V. 2001. *Analysis of Resolution Status Key Technical Issue: Total System Performance Assessment and Integration Subissue 3: Model Abstraction.* Slide presentation at U.S. Nuclear Regulatory Commission/U.S. Department of Energy Technical Exchange and Management Meeting on Total System Performance Assessment and Integration, August 6 through 10, 2001. ACC: MOL.20010921.0129.

CRWMS M&O (Civilian Radioactive Waste Management System Management and Operating Contractor) 2000. *UZ Flow Models and Submodels*. MDL-NBS-HS-000006 REV 00. Las Vegas, Nevada: CRWMS M&O. ACC: MOL.19990721.0527.

Flint, L.E. 1998. *Characterization of Hydrogeologic Units Using Matrix Properties, Yucca Mountain, Nevada*. Water-Resources Investigations Report 97-4243. Denver, Colorado: U.S. Geological Survey. ACC: MOL.19980429.0512.

Gascoyne, M. 2003. "Soluble Salts in the Yucca Mountain Tuff and their Significance." *Proceedings of the 10th International High-Level Radioactive Waste Management Conference (IHLRWM)*, March 30-April 2, 2003, Las Vegas, Nevada. Pages 340-347. La Grange Park, Illinois: American Nuclear Society. TIC: 254202.

Levy, S.S.; Fabryka-Martin, J.T.; Dixon, P.R.; Liu, B.; Turin, H.J.; and Wolfsberg, A.V. 1997. "Chlorine-36 Investigations of Groundwater Infiltration in the Exploratory Studies Facility at Yucca Mountain, Nevada." *Scientific Basis for Nuclear Waste Management XX, Symposium held December 2-6, 1996, Boston, Massachusetts.* Gray, W.J. and Triay, I.R., eds. 465, 901-908. Pittsburgh, Pennsylvania: Materials Research Society. TIC: 238884.

Lu, G.; Sonnenthal, E.L.; and Bodvarsson, G.S. 2003. "Implications of Halide Leaching on 36Cl Studies at Yucca Mountain, Nevada." *Water Resources Research, 39* (12), 1361, 3-1~15, 2003. TIC: 255498.

Montazer, P. and Wilson, W.E. 1984. *Conceptual Hydrologic Model of Flow in the Unsaturated Zone, Yucca Mountain, Nevada*. Water-Resources Investigations Report 84-4345. Lakewood, Colorado: U.S. Geological Survey. ACC: NNA.19890327.0051.

NRC (U.S. Nuclear Regulatory Commission) 2002. *Integrated Issue Resolution Status Report*. NUREG-1762. Washington, D.C.: U.S. Nuclear Regulatory Commission, Office of Nuclear Material Safety and Safeguards. TIC: 253064.

Reamer, C.W. and Gil, A.V. 2001a. *Summary Highlights of NRC/DOE Technical Exchange and Management Meeting on Total System Performance Assessment and Integration.* Meeting held August 6–10, 2001, Las Vegas, Nevada. Washington, D.C.: U.S. Nuclear Regulatory Commission. ACC: MOL.20010921.0121.

Reamer, C.W. and Gil, A.V. 2001b. *Summary Highlights of NRC/DOE Technical Exchange and Management Meeting of Range on Thermal Operating Temperatures, September 18-19, 2001*. Washington, D.C.: U.S. Nuclear Regulatory Commission. ACC: MOL.20020107.0162.

Reamer, C.W. and Williams, D.R. 2000. *Summary Highlights of NRC/DOE Technical Exchange and Management Meeting on Radionuclide Transport held December 5–7, 2000, Berkeley, California*. Washington, D.C.: U.S. Nuclear Regulatory Commission. ACC: MOL.20010117.0063.

Sonnenthal, E.L. and Bodvarsson, G.S. 1999. "Constraints on the Hydrology of the Unsaturated Zone at Yucca Mountain, NV from Three-Dimensional Models of Chloride and Strontium Geochemistry." *Journal of Contaminant Hydrology, 38,* (1-3), 107-156. New York, New York: Elsevier. TIC: 244160.

Wu, Y.S.; Ritcey, A.C.; and Bodvarsson, G.S. 1999. "A Modeling Study of Perched Water Phenomena in the Unsaturated Zone at Yucca Mountain." *Journal of Contaminant Hydrology, 38,* (1-3), 157-184. New York, New York: Elsevier. TIC: 244160.